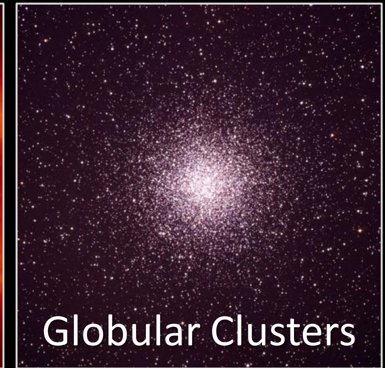

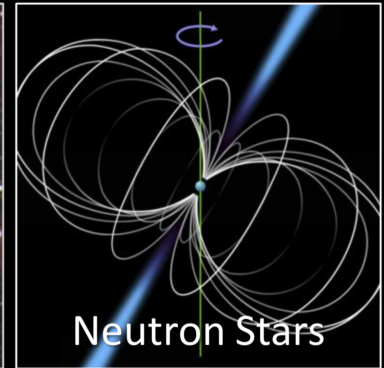

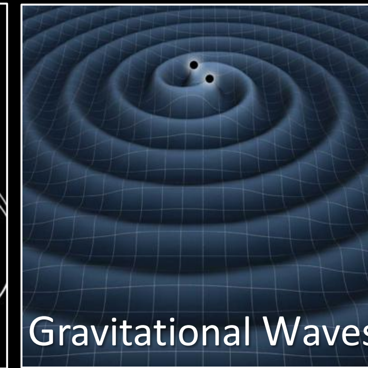

Axion Bounds from Stars

Barolo Astroparticle Meeting, 12–15 June 2024

ORIGINS Excellence Cluster

COSMIC WISPERS CA21106

Max-Planck-Institut für Physik (Werner-Heisenberg-Institut)

SFB 1258 | Neutrinos Dark Matter Messengers

Georg G. Raffelt, Max-Planck-Institut für Physik, Garching

Astrophysical Axion Bounds and Opportunities

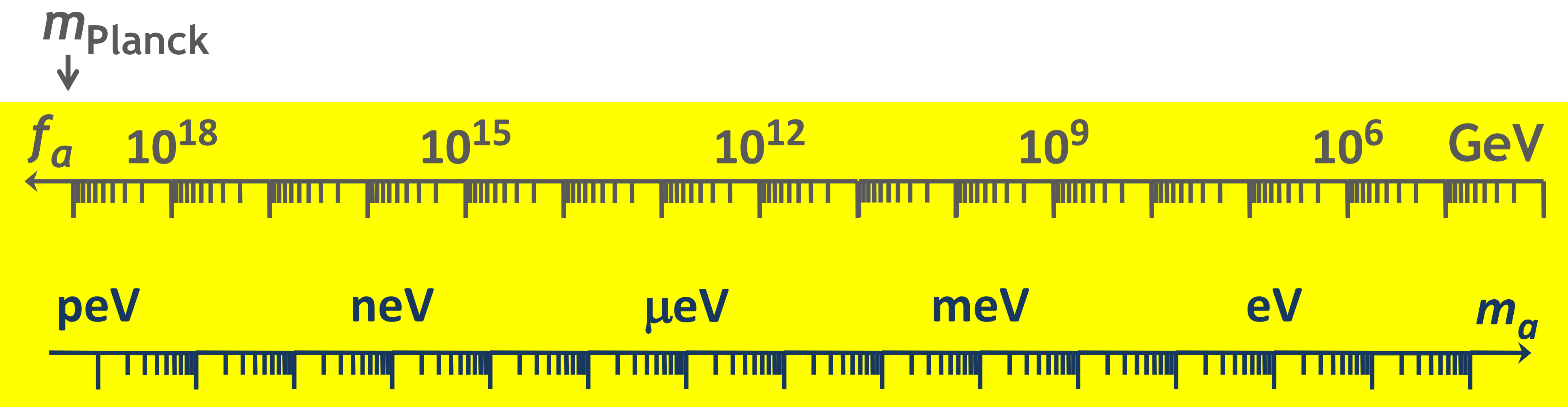

Super Radiance

Opportunities for detection

Astrophysical Bounds (Energy loss of stars)

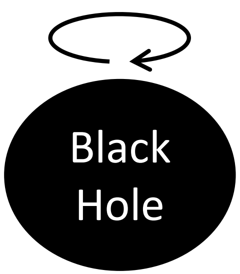

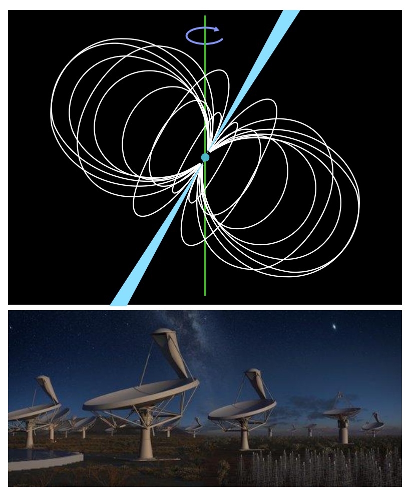

Axion conversion in neutron star magnetospheres

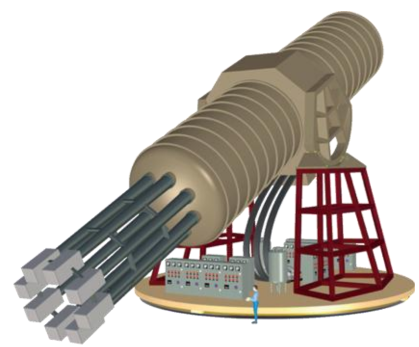

IAXO Solar Axion Telescope

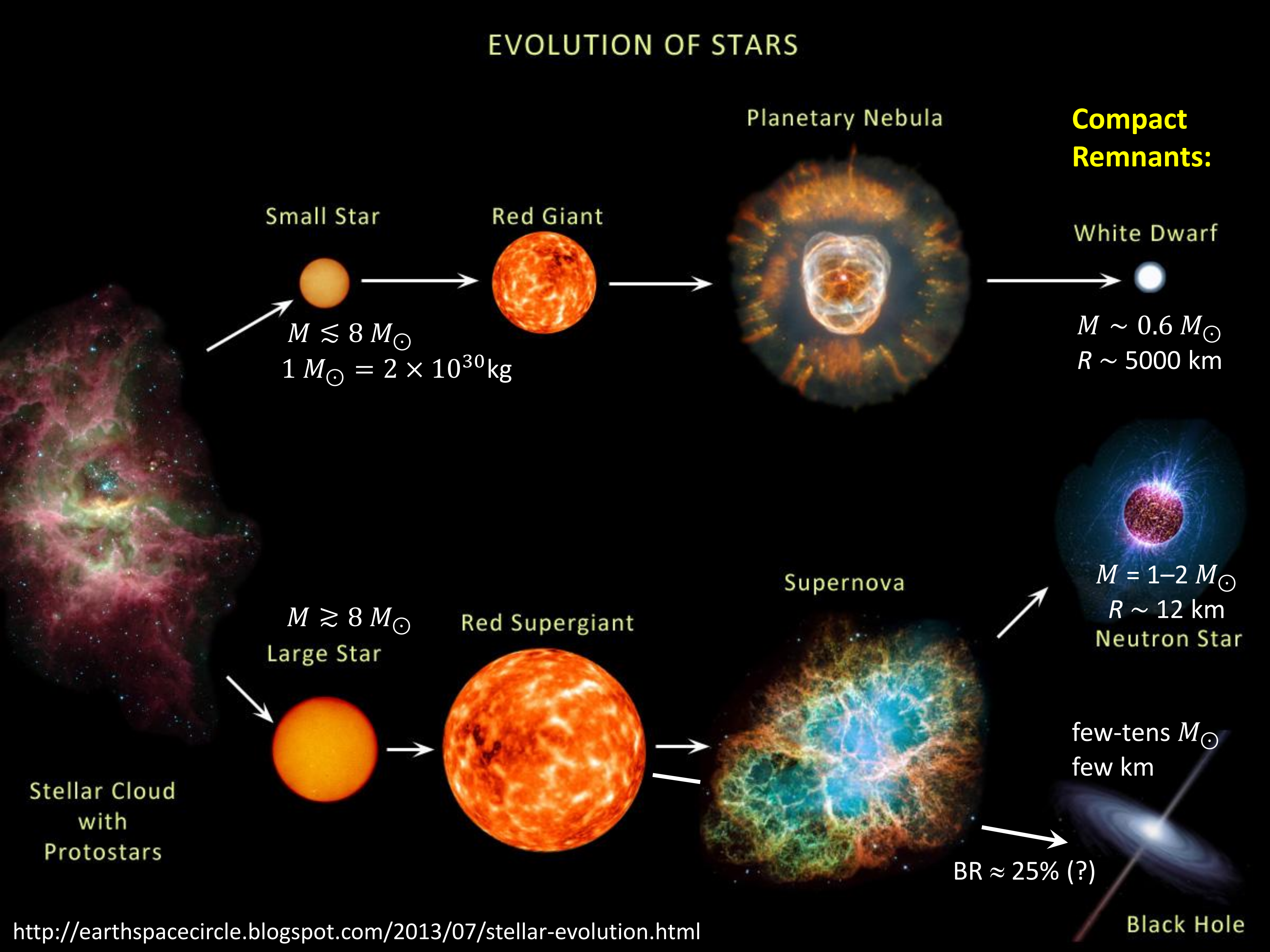
EVOLUTION OF STARS
Small Star
Red Giant
Planetary Nebula
Compact Remnants:
White Dwarf
$M \lesssim 8\ M_\odot$
$1\ M_\odot = 2 \times 10^{30}$kg
$M \sim 0.6\ M_\odot$
$R \sim 5000$ km
$M = 1\text{–}2\ M_\odot$
$R \sim 12$ km
Neutron Star
Supernova
$M \gtrsim 8\ M_\odot$
Large Star
Red Supergiant
few-tens $M_\odot$
few km
Stellar Cloud with Protostars
BR ≈ 25% (?)
Black Hole
http://earthspacecircle.blogspot.com/2013/07/stellar-evolution.html

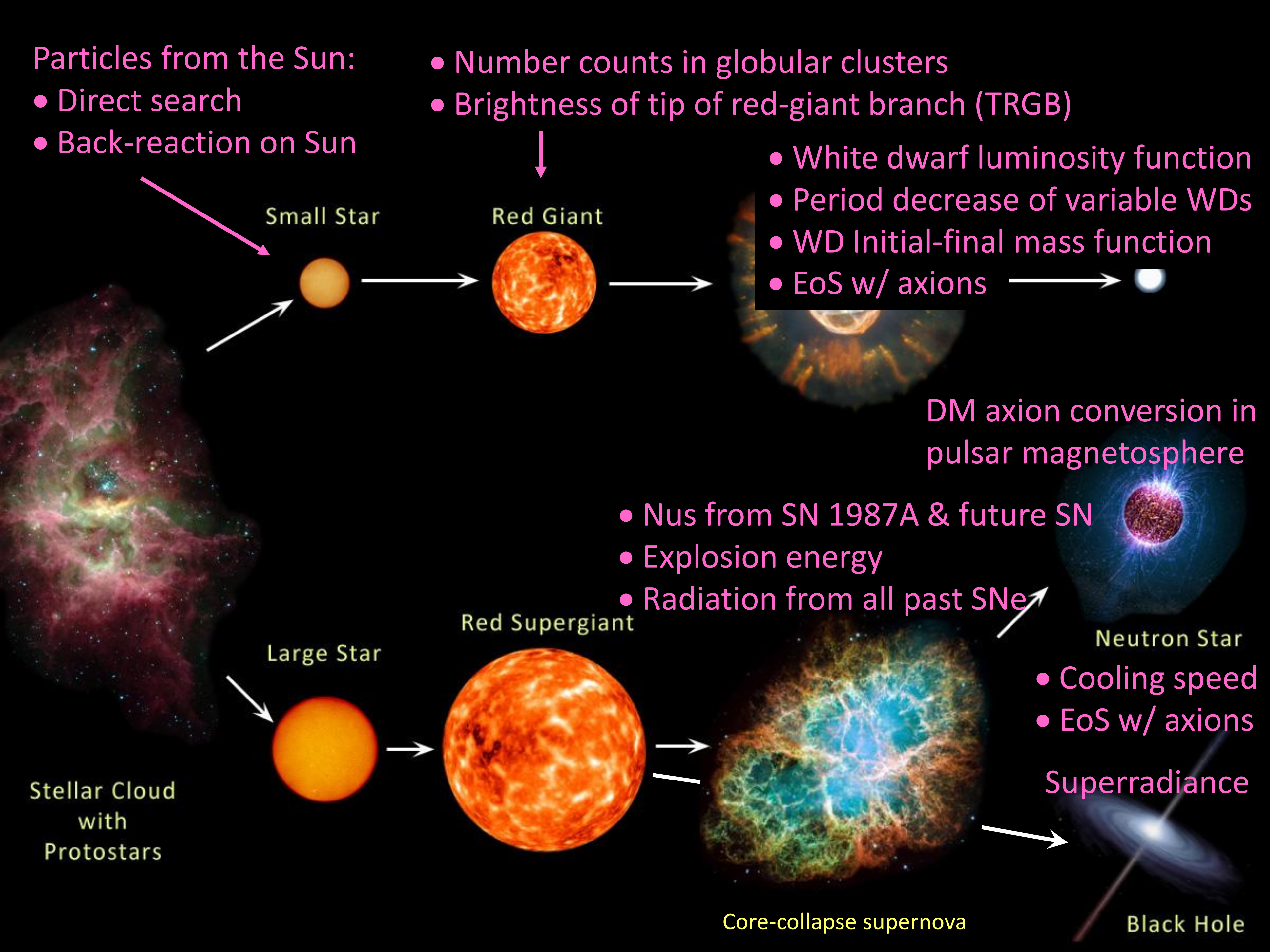
Particles from the Sun:
• Direct search
• Back-reaction on Sun
• Number counts in globular clusters
• Brightness of tip of red-giant branch (TRGB)
• White dwarf luminosity function
• Period decrease of variable WDs
• WD Initial-final mass function
• EoS w/ axions
Small Star
Red Giant
DM axion conversion in pulsar magnetosphere
• Nus from SN 1987A & future SN
• Explosion energy
• Radiation from all past SNe
Neutron Star
• Cooling speed
• EoS w/ axions
Large Star
Red Supergiant
Superradiance
Stellar Cloud with Protostars
Core-collapse supernova
Black Hole

Hertzsprung Russell Diagram

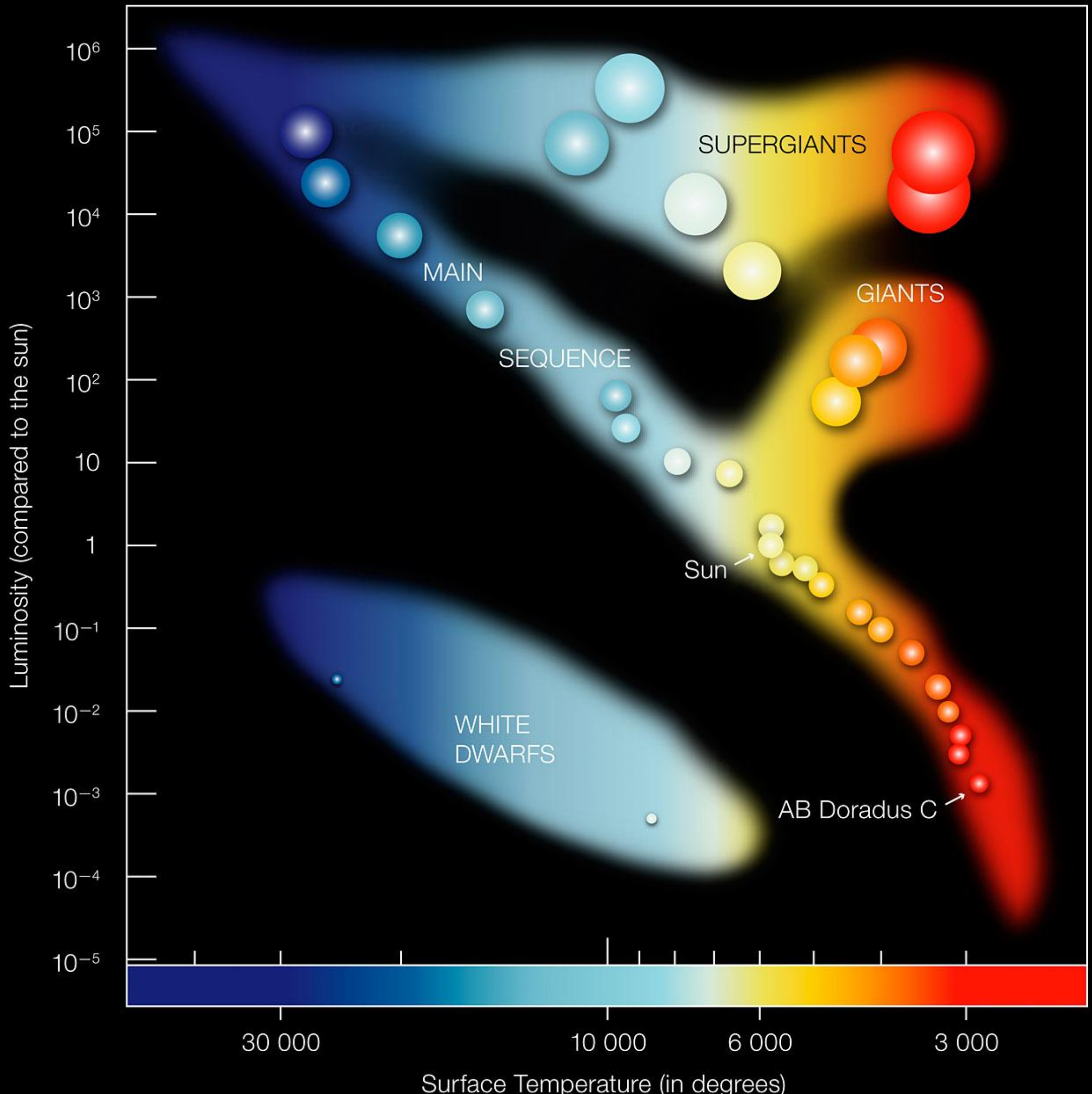

https://www.eso.org/public/images/eso0728c/

Grand Unified ALP Scape

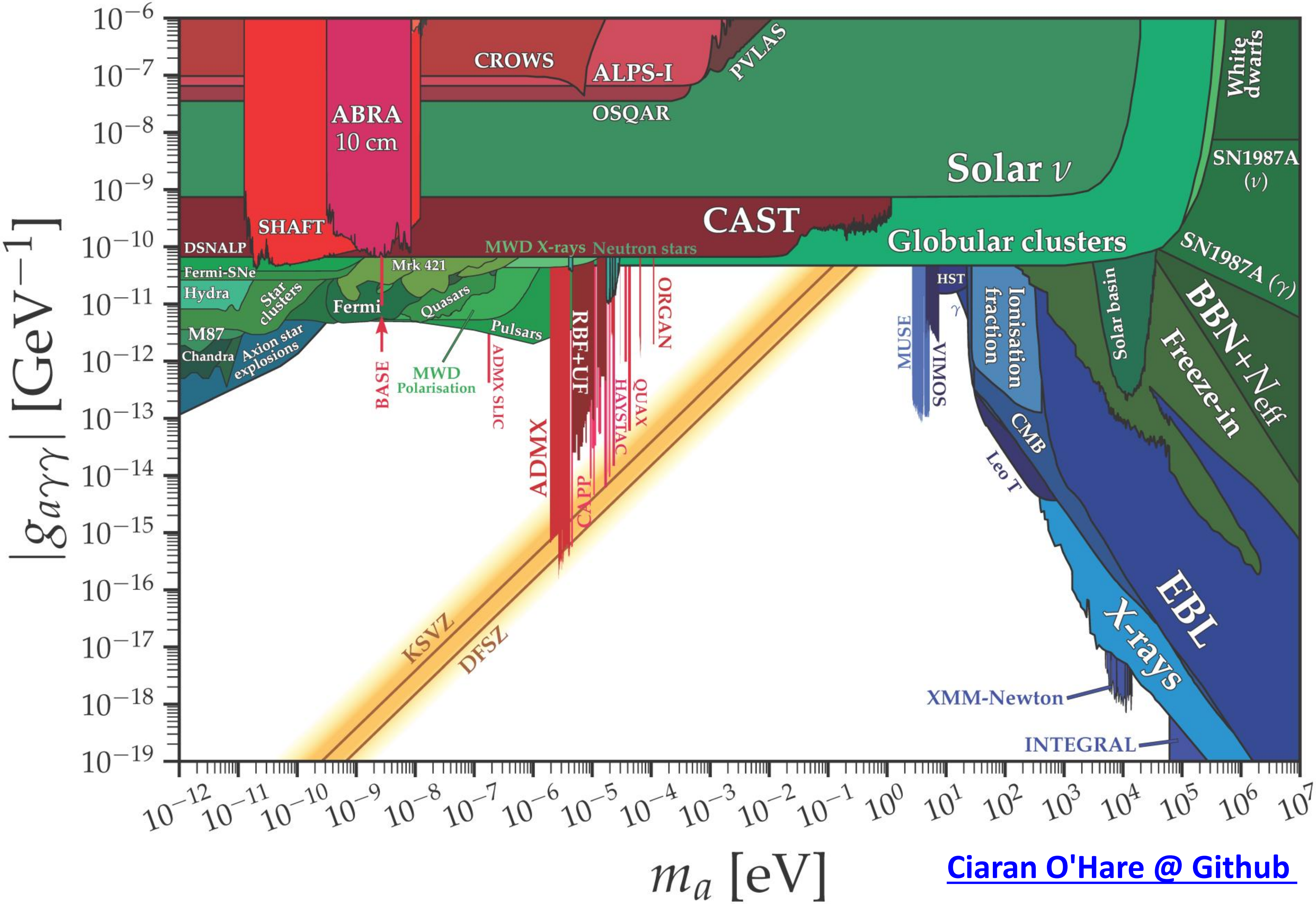

Ciaran O'Hare @ Github

Galactic Globular Cluster M55

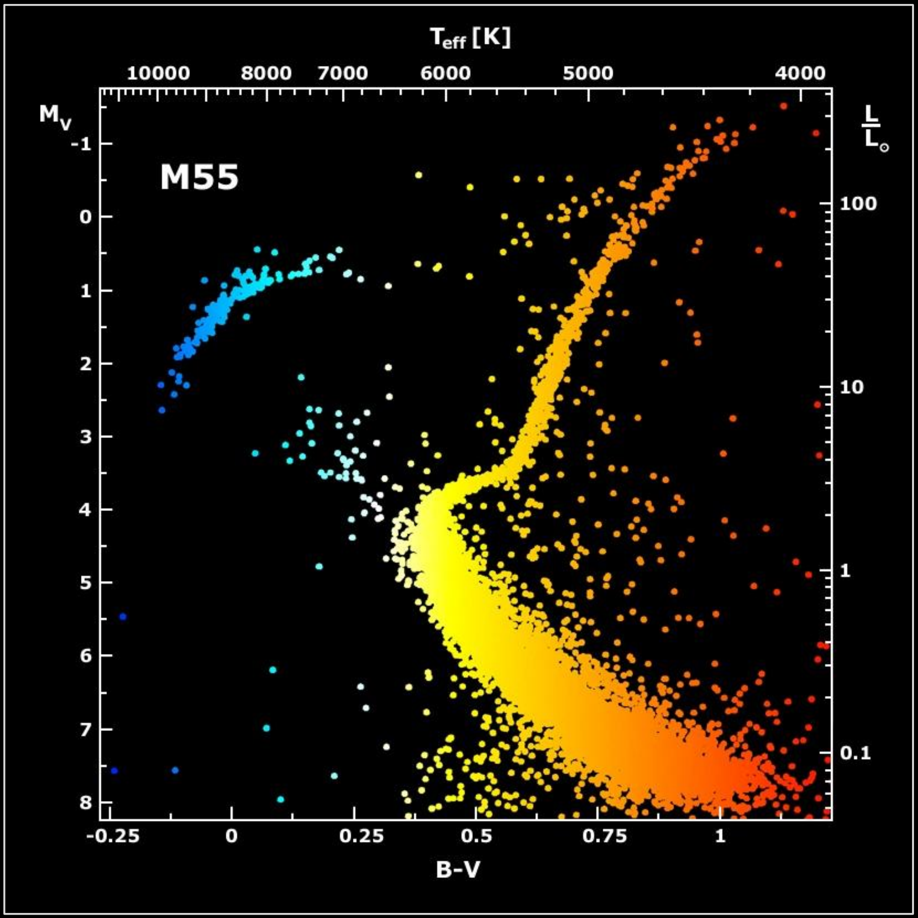

Color-Magnitude Diagram for Globular Clusters

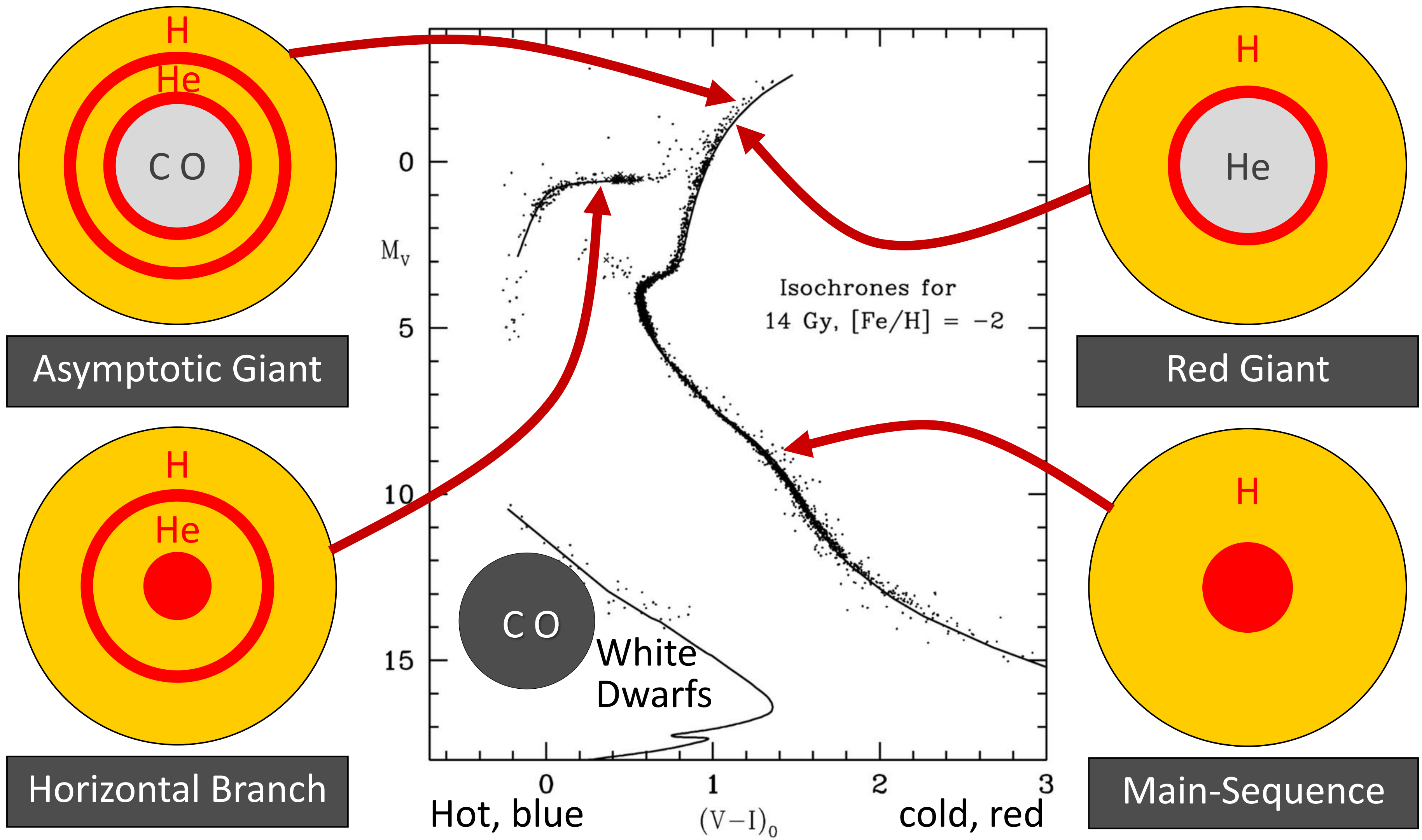

Color-magnitude diagram synthesized from several low-metallicity globular clusters and compared with theoretical isochrones (W.Harris, 2000)

Color-Magnitude Diagram for Globular Clusters

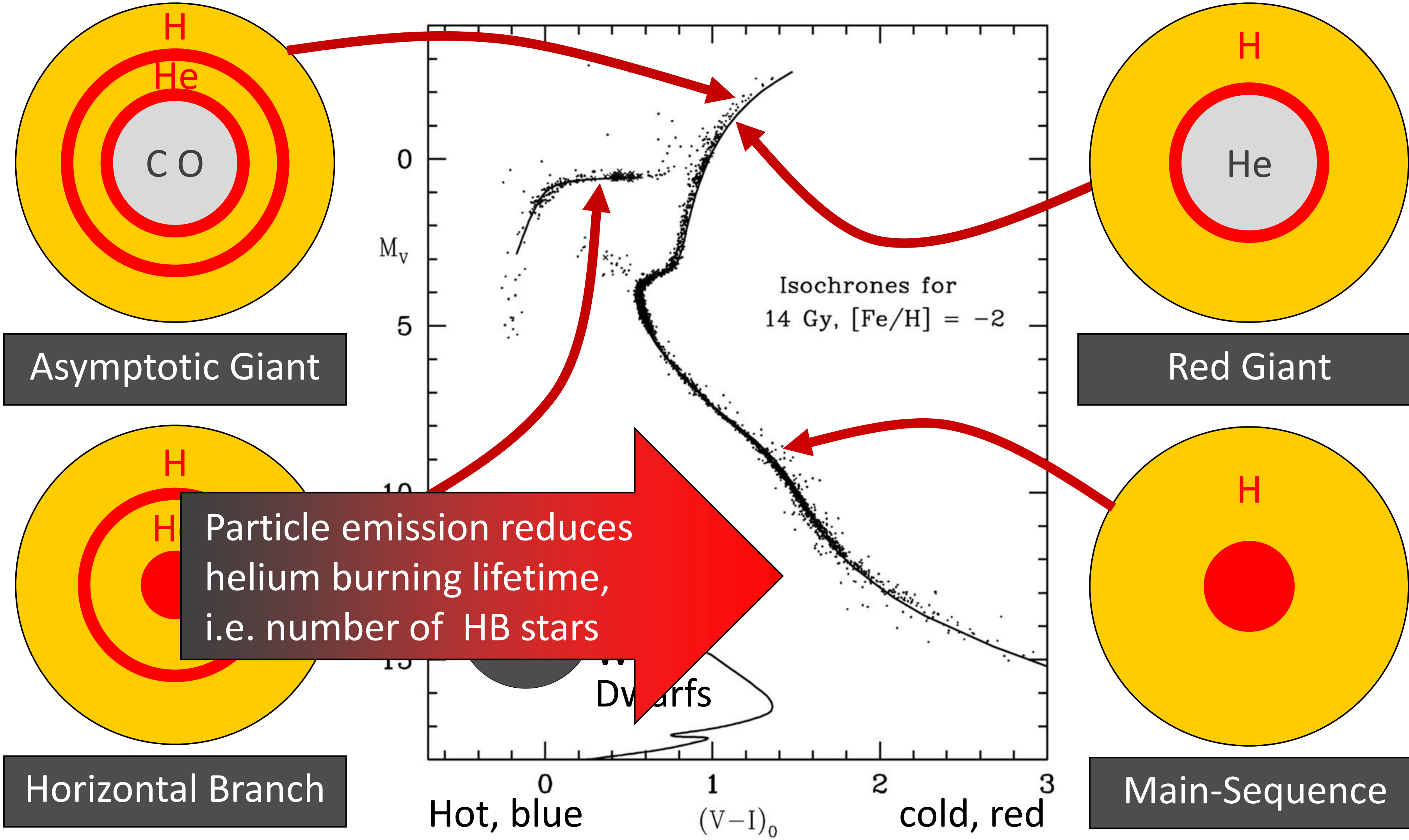

Color-magnitude diagram synthesized from several low-metallicity globular clusters and compared with theoretical isochrones (W.Harris, 2000)

Helium Burning Lifetime: R-Method

Number ratio ("R") of HB/RGB fixes He-burning lifetime
(if RGB not affected by new energy loss)

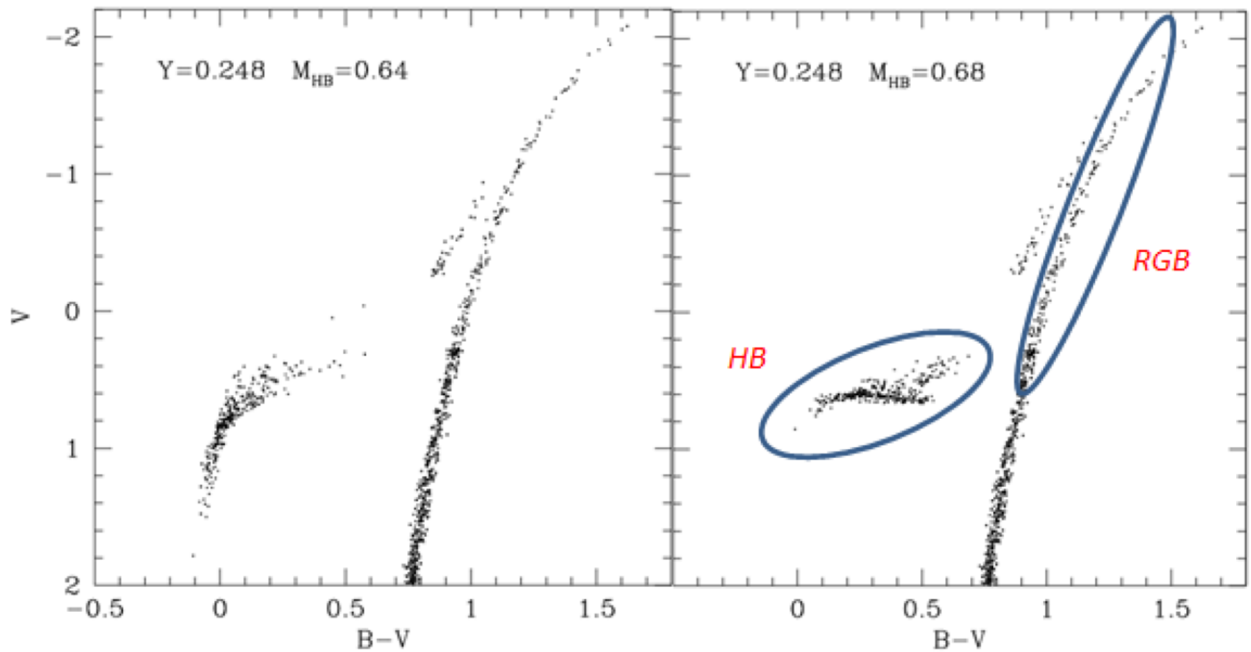

Figure 1: Example of synthetic CM diagrams. The diagram in the left panel has been obtained by assuming a stronger average mass loss rate during the RGB. As a result, the mean mass of HB stars (M_{HB}) is lower than that of the diagram in the right panel. The HB and the RGB portions used in the calculation of the R parameter are surrounded by ellipses.

Straniero, Ayala, Giannotti, Mirizzi & Domínguez,
doi:10.3204/DESY-PROC-2015-02/straniero_oscar

ALP Limits from Globular Clusters

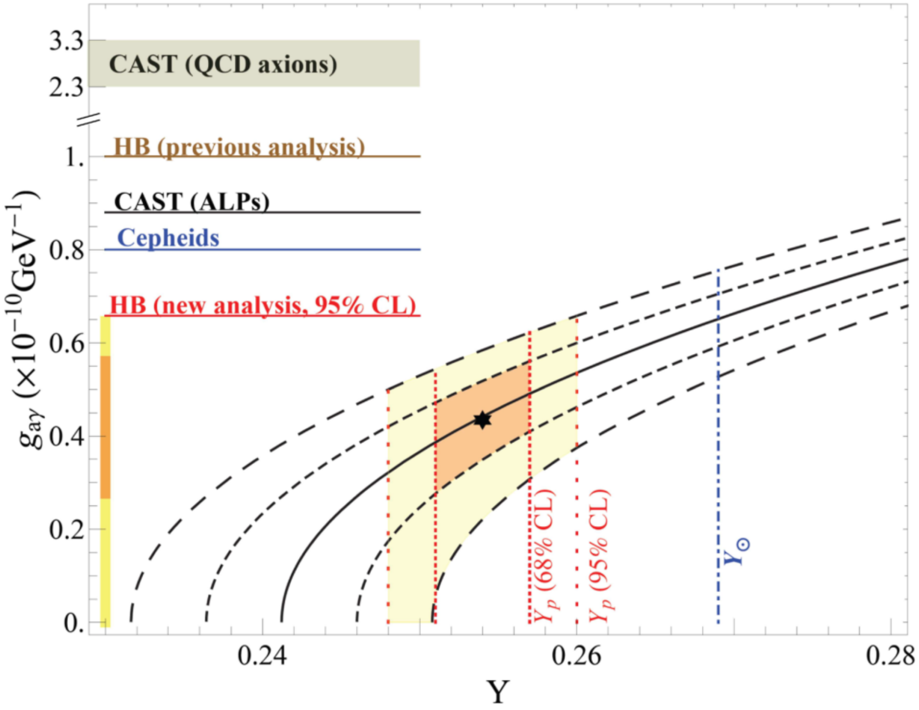

Parameter	error	Reference
$^{14}N(p,\gamma)^{15}O$	7%	[1]
$^{4}He(2\alpha,\gamma)^{12}C$	10%	[2]
$^{12}C(\alpha,\gamma)^{16}O$	20%	[6]
R	1.39 ± 0.03	[4]
Y	0.255 ± 0.002	[5],[3]

Helium abundance and energy loss rate from modern number counts HB/RGB in 39 globular clusters R = 1.39 ± 0.03

$$R_{\rm th} = 1.48 + 6.26(Y - 0.255) - 0.41 g_{10}^2$$

$$g_{a\gamma} < 0.66 \times 10^{-10}\,\mathrm{GeV}^{-1}$$ **(95% CL)**

Same as CAST limit within 2 digits ☺

Small "cooling hint" almost certainly systematics (as usual in astrophysics) eg nuclear reaction rates
Need more systematic exploration of systematics!

Ayala, Dominguez, Giannotti, Mirizzi & Straniero, arXiv:1406.6053
doi:10.3204/DESY-PROC-2015-02/straniero_oscar
Update including ALP masses: Lucente, Straniero, Carenza, Giannotti & Mirizzi, arXiv:2203.01336

AGB/HB Counts in 48 Globular Clusters

NGC	[Fe/H]	$L1$	$L2$	Piotto et al. (2002)			Sarajedini et al. (2007)			Sandquist (2000)		
				n_{HB}	n_{AGB}	R_2	n_{HB}	n_{AGB}	R_2	n_{HB}	n_{AGB}	R_2
104	-0.72	0.078	0.068	358	53	0.148	591	82	0.139	368	38	0.103
362	-1.26	0.086	0.608	238	40	0.168	318	43	0.135	94	14	0.149
1261	-1.27	0.088	0.644	94	22	0.234	233	34	0.146	148	26	0.176
1851	-1.18	0.098	0.679	272	37	0.136	411	49	0.119	209	24	0.115
1904	-1.60	...	...	163	11	0.067	...	...	...	122	16	0.131
2419	-2.15	0.192	0.852	225	22	0.098	...	...	...	...	...	...
2808	-1.14	0.094	0.904	809	61	0.075	1200	104	0.087	247	22	0.089
4833	-1.85	0.287	0.538	94	10	0.106	...	...	...	...	...	...
5024	-2.10	0.158	0.602	224	18	0.080	360	44	0.122	302	39	0.129
5272	-1.50	0.150	0.613	...	...	...	323	40	0.124	562	65	0.116
5634	-1.88	...	...	130	15	0.115	...	...	...	...	...	...
5694	-1.98	...	...	222	26	0.117	...	...	...	56	14	0.250
5824	-1.91	...	...	463	63	0.136	...	...	...	...	...	...
5904	-1.29	0.150	0.681	162	21	0.130	280	52	0.186	555	94	0.169
5927	-0.49	0.043	0.062	201	12	0.060	...	...	...	134	20	0.149
6093	-1.75	0.464	0.447	162	31	0.191	341	51	0.150	170	39	0.229
6139	-1.65	...	...	282	35	0.124	...	...	...	114	24	0.211
6171	-1.02	0.100	0.513	...	...	...	56	10	0.179	117	29	0.248
6205	-1.53	0.527	0.441	192	20	0.104	390	48	0.123	90	12	0.133
6218	-1.47	0.561	0.299	...	...	...	82	11	0.134	91	12	0.132
6229	-1.18	...	...	278	34	0.122	...	...	...	92	19	0.207
6254	-1.26	0.588	0.260	...	...	...	157	18	0.115	69	13	0.188
6266	-1.18	...	...	446	40	0.090	...	...	...	114	18	0.158
6284	-1.26	...	...	127	16	0.126	...	...	...	...	...	...
6304	-0.45	0.062	0.060	99	8	0.081	...	...	...	...	...	...
6341	-2.31	0.261	0.542	...	...	...	245	33	0.135	140	20	0.143
6356	-0.40	...	...	362	25	0.069	...	...	...	...	...	...
6362	-0.59	0.122	0.621	38	6	0.158	...	...	...	...	...	...
6388	-0.55	0.057	0.836	1347	176	0.131	...	...	...	...	...	...
6402	-1.28	...	...	349	29	0.083	...	...	...	...	...	...
6441	-0.46	0.048	0.904	1380	154	0.112	...	...	...	...	...	...
6539	-0.63	...	...	114	15	0.132	...	...	...	...	...	...
6541	-1.81	0.563	0.347	...	...	...	248	41	0.165	...	...	...
6569	-0.76	...	...	166	30	0.181	...	...	...	...	...	...
6584	-1.50	0.102	0.558	55	8	0.145	...	...	...	...	...	...
6624	-0.44	0.077	0.085	121	9	0.074	188	20	0.106	126	30	0.238
6637	-0.64	0.078	0.065	135	25	0.185	244	43	0.176	127	21	0.165
6638	-0.95	...	...	101	28	0.277	...	...	...	...	...	...
6652	-0.81	0.073	0.080	61	5	0.082	83	9	0.108	75	20	0.267
6681	-1.62	0.558	0.334	100	9	0.090	...	...	...	82	8	0.098
6723	-1.10	0.127	0.704	102	11	0.108	194	22	0.113	101	15	0.149
6752	-1.54	0.378	0.578	...	...	...	173	20	0.116	225	13	0.058
6864	-1.29	...	...	363	69	0.190	...	...	...	55	12	0.218
6934	-1.47	0.097	0.678	149	18	0.121	99	17	0.172	...	...	...
6981	-1.42	0.142	0.570	61	7	0.115	188	36	0.191	45	10	0.222
7078	-2.37	0.174	0.713	376	48	0.128	537	57	0.106	153	23	0.150
7089	-1.65	0.150	0.790	167	18	0.108	702	100	0.142	...	...	...
7099	-2.27	0.462	0.261	89	6	0.067	...	...	...	202	11	0.054

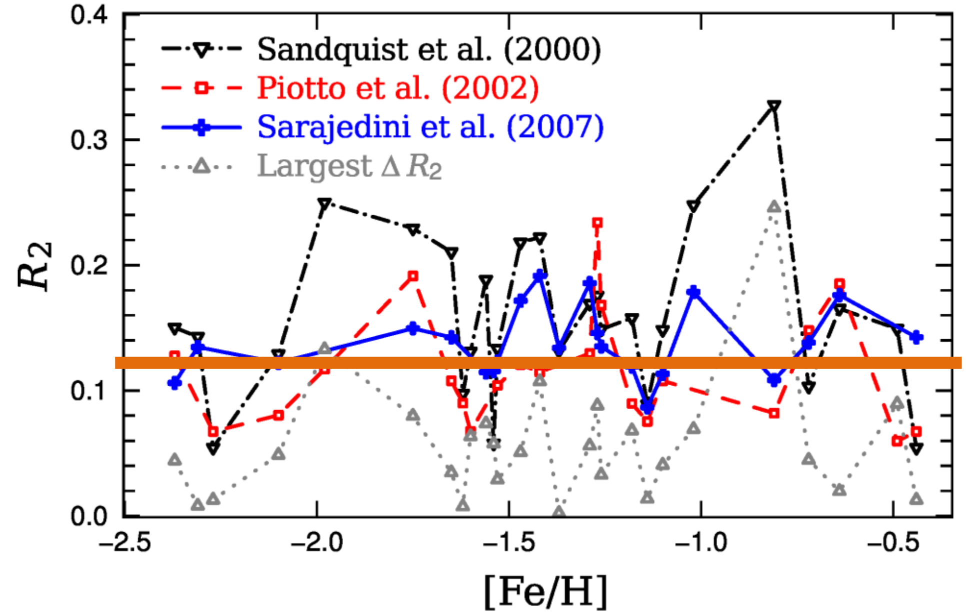

Figure 1. Comparison of R_2 for clusters shown in Table 1, limited to those with at least two different sources of photometry. The R_2 determined from the Sandquist (2000), Piotto et al. (2002), and Sarajedini et al. (2007) data are shown in black dash-dots, red dashes, and a blue solid line, respectively. The dotted grey line shows the maximum difference between R_2 determinations from different photometry.

$R_2 = N_{AGB}/N_{HB} = 0.117 \pm 0.005$

The treatment of mixing in core helium burning models II. Constraints from cluster star counts
Constantino, Campbell, Lattanzio & van Duijneveldt, arXiv:1512.04845

HB vs. AGB Clump on Luminosity Function

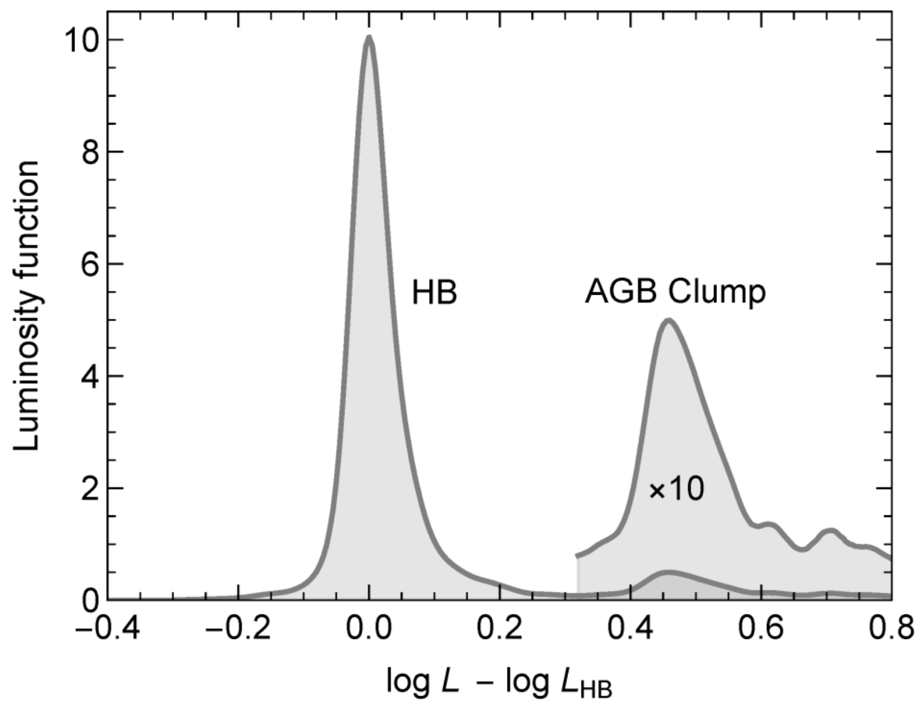

Figure 8: Empirical luminosity function, normalized to one, of the HB plus AGB stars from 14 GCs without a blue extension of the HB [212], using HST photometric data of Piotto et al. [213] and Sarajedini et al. [214]. We show a superposition of the two curves of Fig. 6 of [212], weighted with the number of stars (2414 for Sarajedini et al. and 4036 for Piotto et al.), although there is large overlap between the used clusters. Each one was aligned to its HB luminosity, defined as the maximum of the distribution. The AGB clump at $\log L - \log L_{\rm HB} = 0.455$ sticks out as a narrow peak. The separation between HB and AGB is taken at the minimum between the peaks, and the AGB itself until $\log L - \log L_{\rm HB} = 1$. A total of 725 AGB and 5725 HB stars went into the construction of this distribution, corresponding to $R_2 = 0.127$ for the clusters that went into this plot.

Predicting the Axion-Modified Ratios

M.J. Dolan, F.J. Hiskens & R.R. Volkas, arXiv:2207.03102

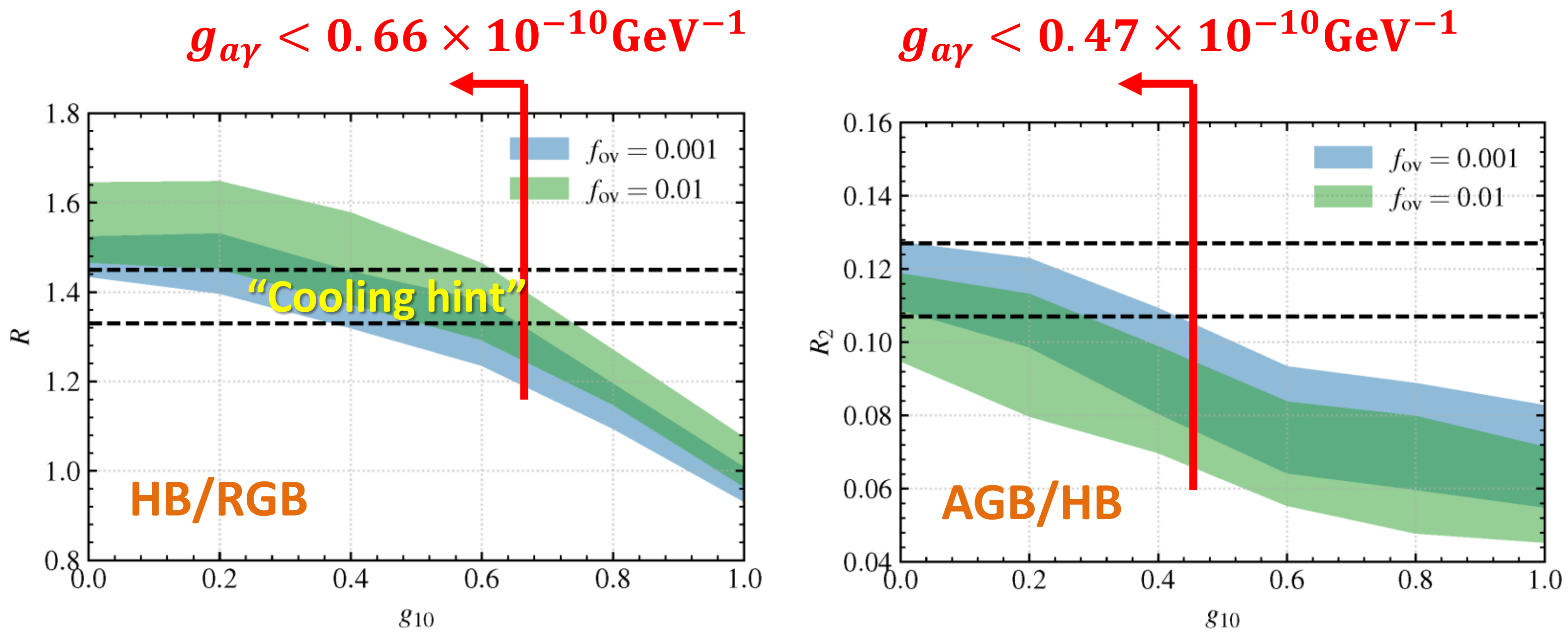

Figure 2. (Left panel): Predicted values of R as a function of g_{10} given standard convective core overshoot with $f_{ov} = 0.001$ (blue) and $f_{ov} = 0.01$ (green). The observed limit on R is indicated by the region between the dashed black lines (95% C.I.). (Right panel): The full range of R_2 values predicted as functions of g_{10} given standard overshoot with $f_{ov} = 0.001$ (blue) and $f_{ov} = 0.01$ (green). The observed limit is again shown by the dashed black lines.

Probably one should analyze GCs for all observables simultaneously using modern high-statistics (GAIA) data

Role of Core Breathing Pulses at End of He Burning

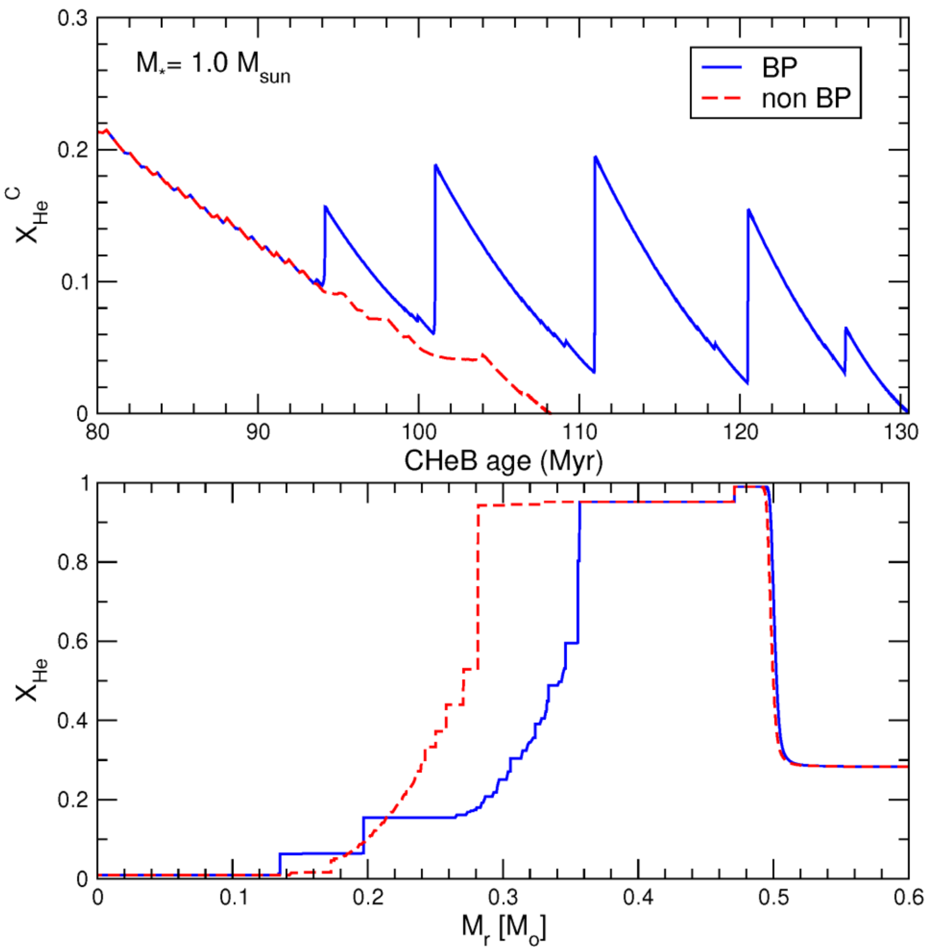

Figure 1. Upper panel: core He abundance (by mass) in terms of the CHeB age. Solid (dashed) line corresponds to the case in which BPs during the CHeB phase have been allowed (suppressed). Bottom panel: inner He abundance distribution at the end of CHeB phase when the central He abundance is $X_{\rm He} \approx 0.01$ for the two situations illustrated in the upper panel.

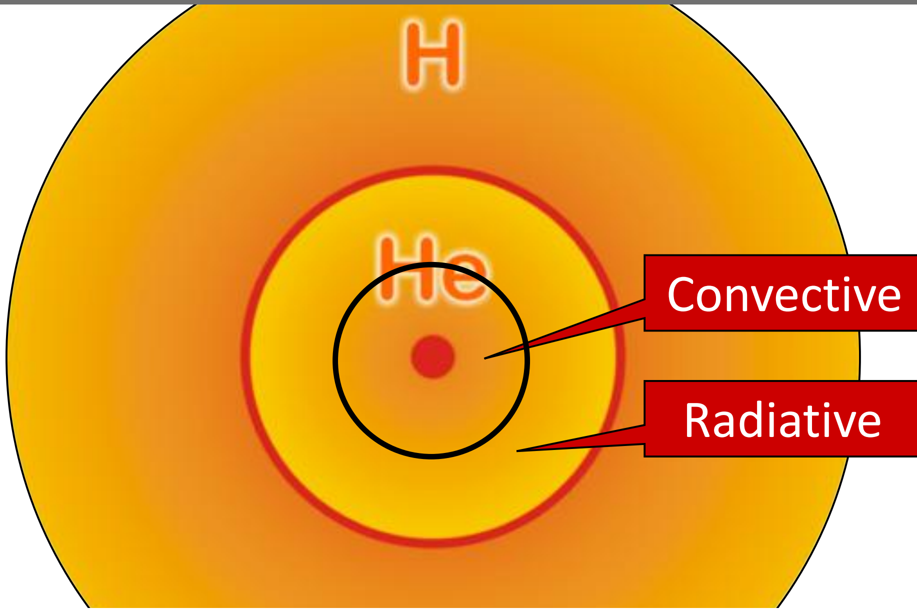

- He-burning core convective
- At the end unstable edge "core breathing pulses" (BP)
- Usually suppressed "by hand" in evolution simulations
- Strong impact on number ratios and later white dwarf stage

[Córsico & Althaus, arXiv:2402.03490]

Gaia DR2: Observational Hertzsprung-Russell Diagrams

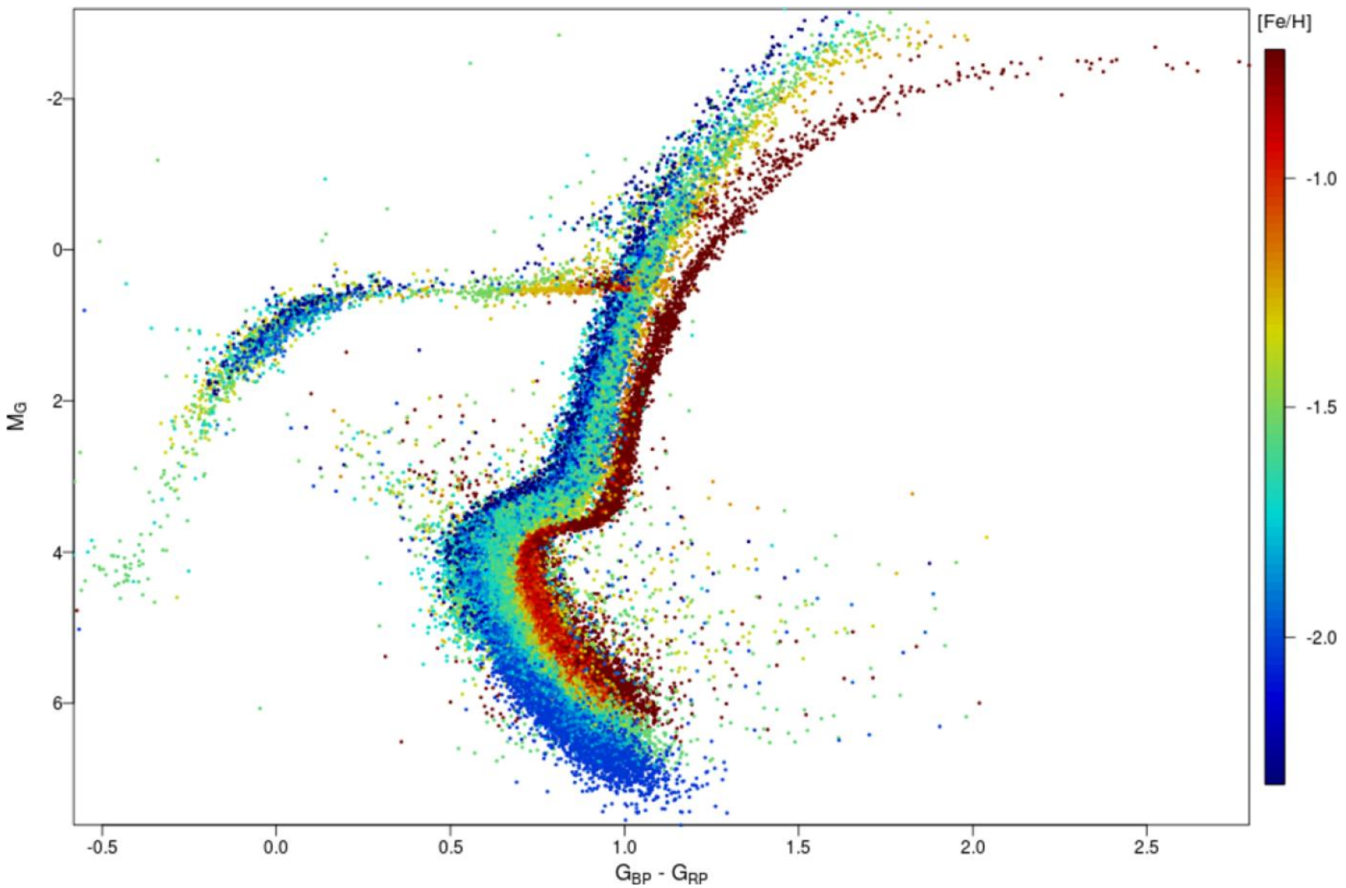

ESA's Gaia Satellite
2013–2025(?)
Unprecedeted astrometric survey

Composite HRD for 14 globular clusters, coloured according to metallicity

arXiv:1804.09378

Color-Magnitude Diagram for Globular Clusters

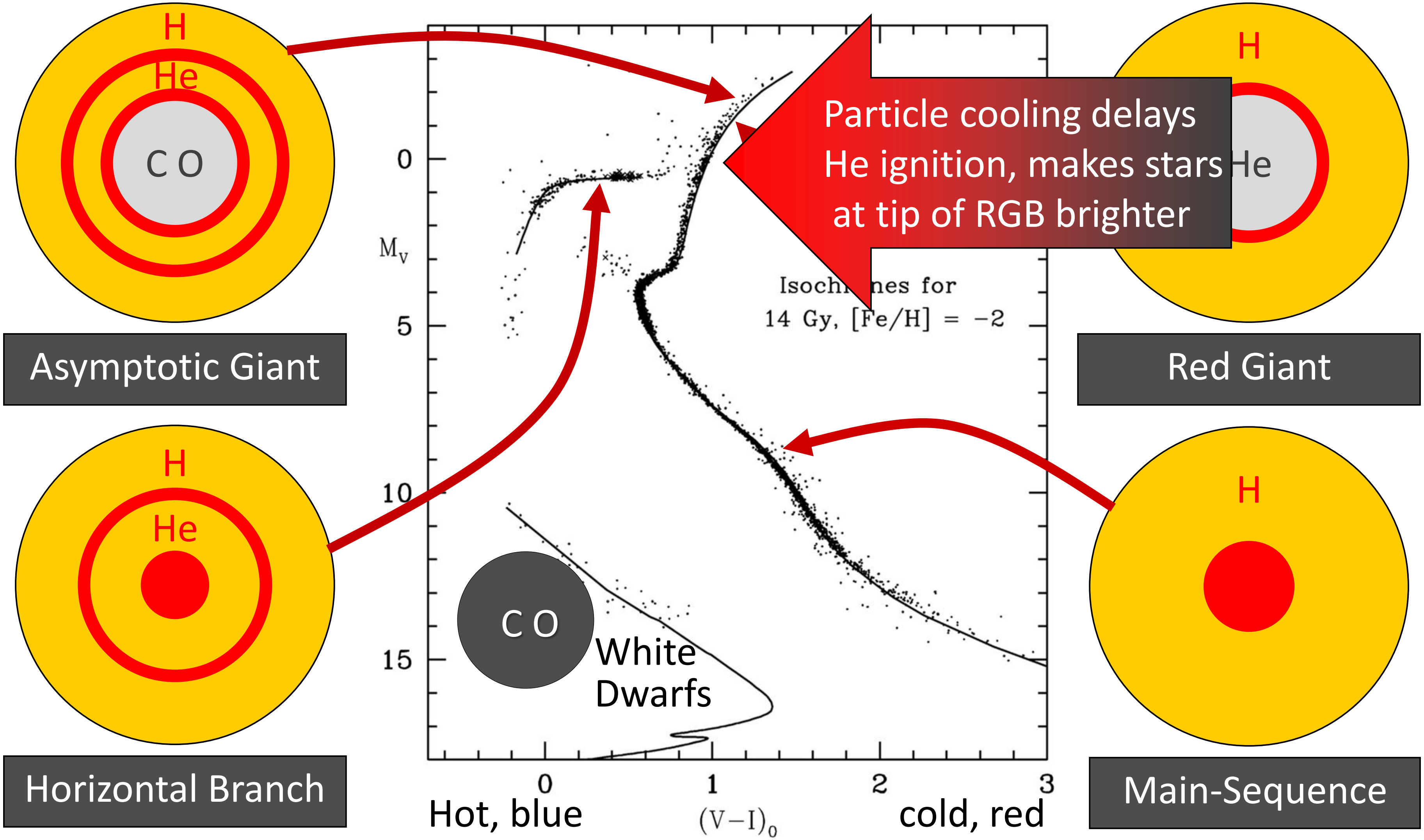

Color-magnitude diagram synthesized from several low-metallicity globular clusters and compared with theoretical isochrones (W.Harris, 2000)

Color-Magnitude Diagram for Globular Clusters

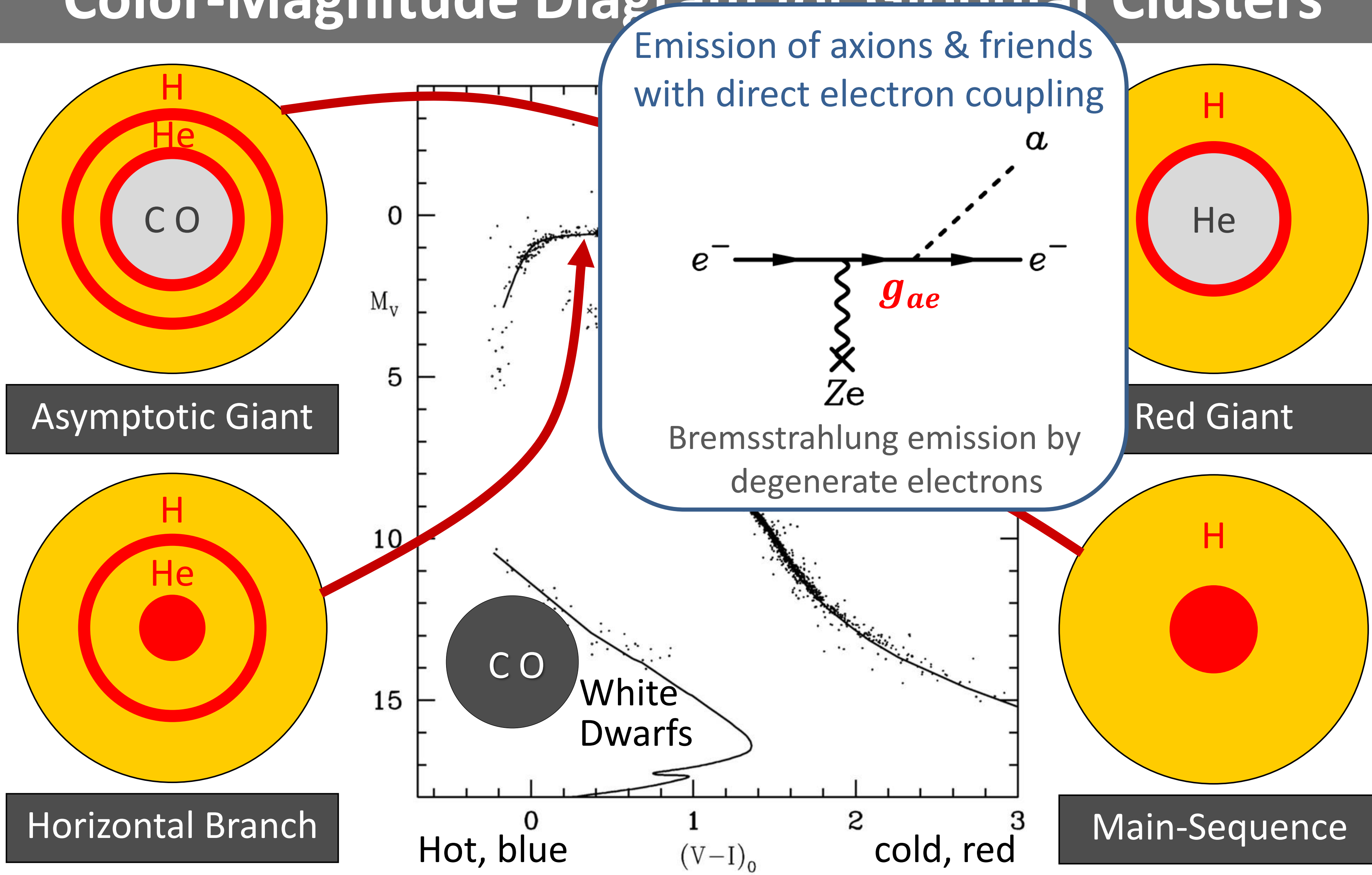

Color-magnitude diagram synthesized from several low-metallicity globular clusters and compared with theoretical isochrones (W.Harris, 2000)

TRGB in 46 Globular Clusters [Cerny+ 2012.09701]

New TRGB Calibration from 21 Globular Clusters

Straniero+ arXiv:2010.03833 and https://www.ggi.infn.it/talkfiles/slides/slides6554.pdf

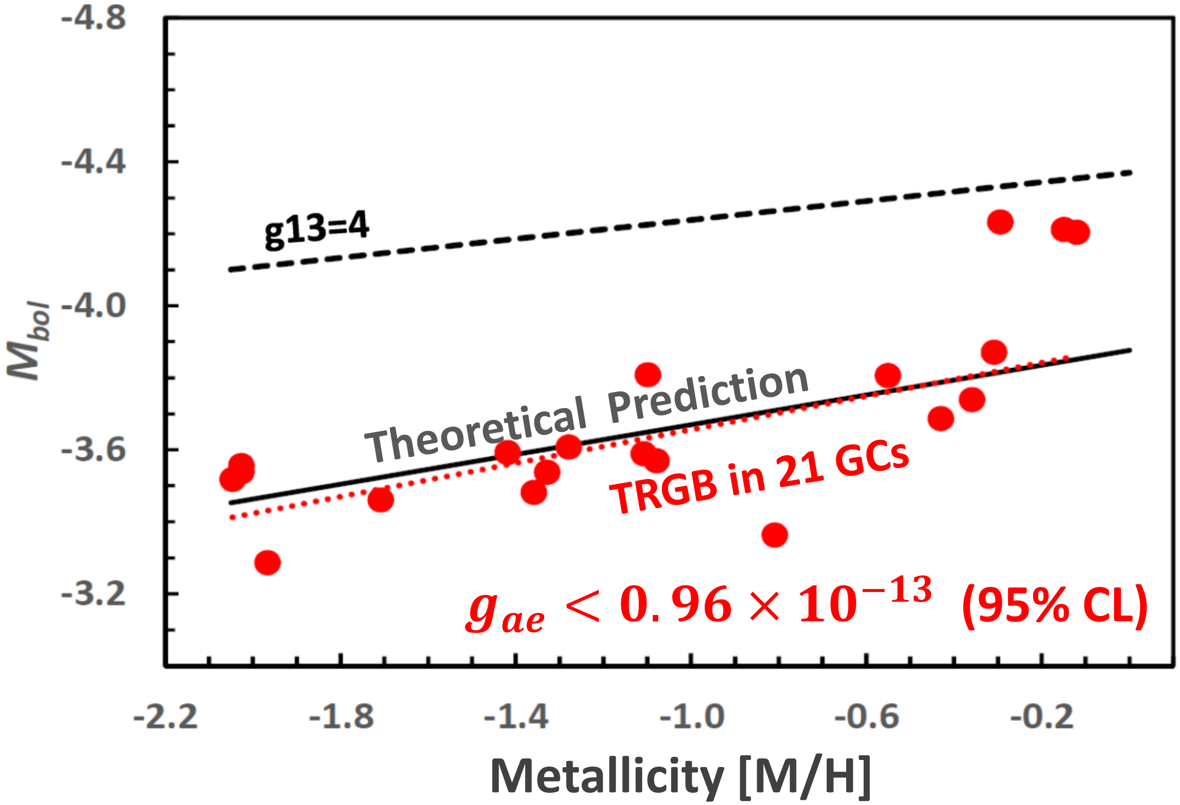

Emission of axions & friends with direct electron coupling

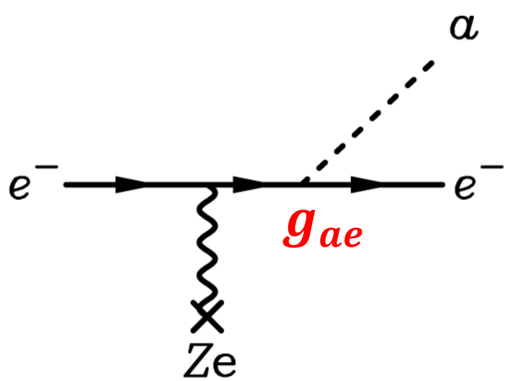

Bremsstrahlung emission by degenerate electrons

DFSZ Axions

$$m_a = 6\ \mathrm{meV}\,\frac{10^9\mathrm{GeV}}{f_a} \qquad g_{ae} = \frac{m_e C_e}{f_a}$$

$$\mathcal{L}_{ae} = \frac{C_e}{2f_a}\bar{e}\gamma^\mu\gamma_5 e\,\partial_\mu a \qquad C_e = \frac{\cos^2\beta}{3}$$

$$\frac{f_a}{\cos^2\beta} > 1.8 \times 10^9\ \mathrm{GeV}$$

Tip of the Red-Giant Branch in the Galaxy NGC 4258

THE ASTROPHYSICAL JOURNAL, 835:28 (17pp), 2017 January 20 JANG & LEE

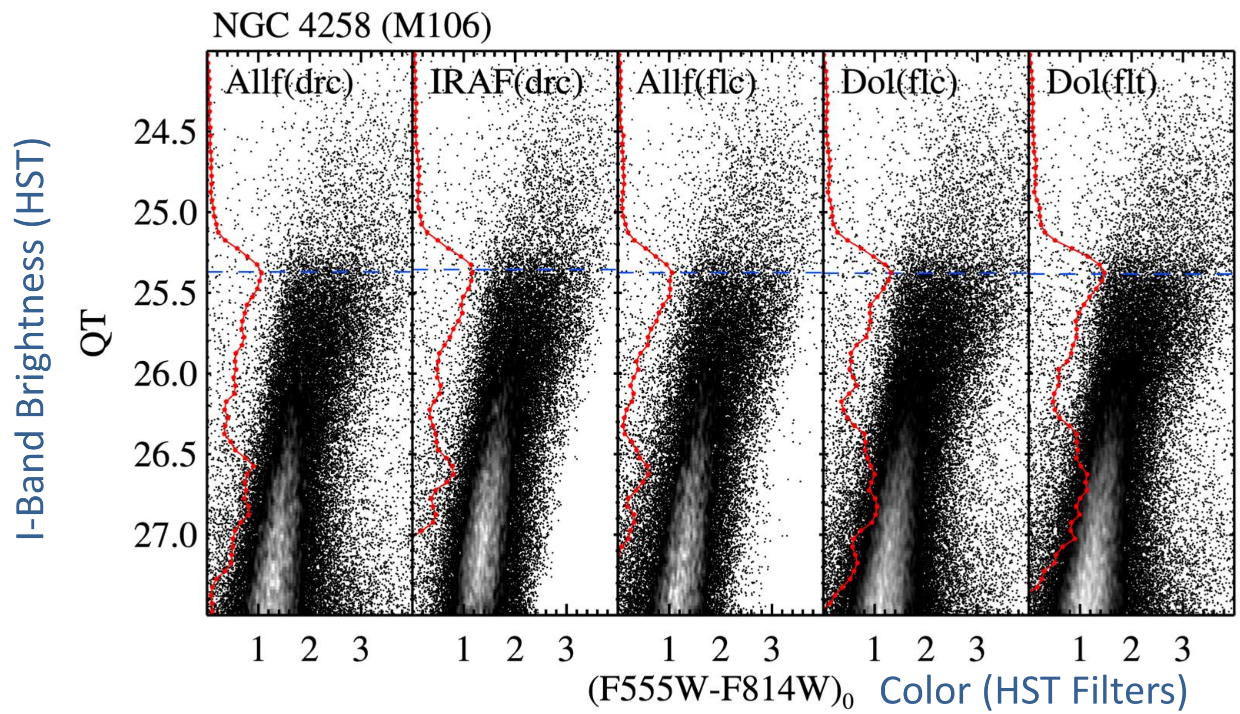

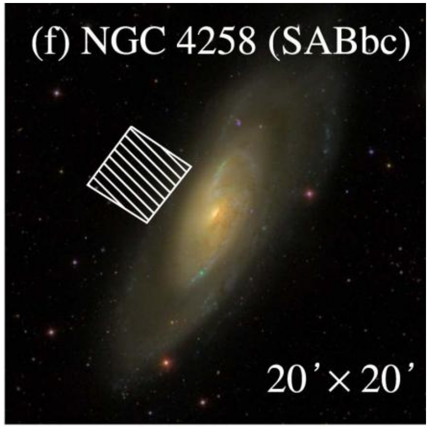

Figure 7. QT − (F555W − F814W)$_0$ CMDs of NGC 4258 from five different reduction methods : ALLFRAME on drc, IRAF/DAOPHOT on drc, ALLFRAME on flc, DOLPHOT on flc, and DOLPHOT on flt (from left to right). Edge detection responses are shown by the solid lines. Note that the estimated TRGB magnitudes (dashed lines) agree very well.

NGC 4258 hosts a water megamaser
→ Quasi-geometric distance determination
→ Among the best absolute TRGB calibrations

Hubble Tension

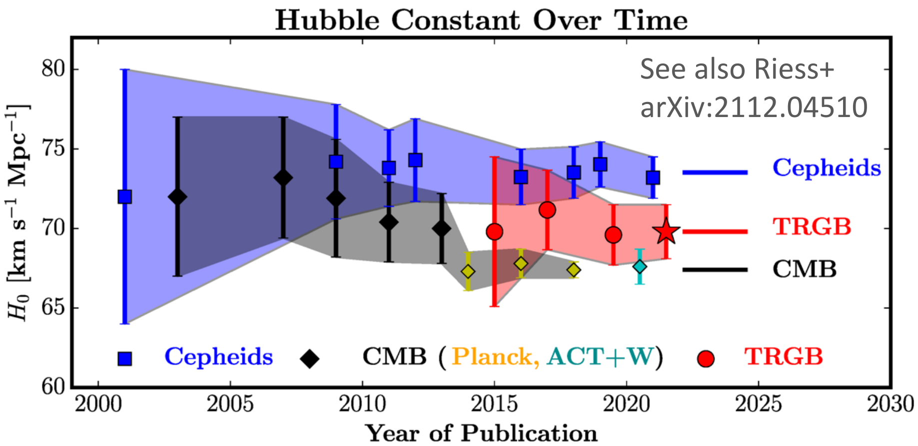

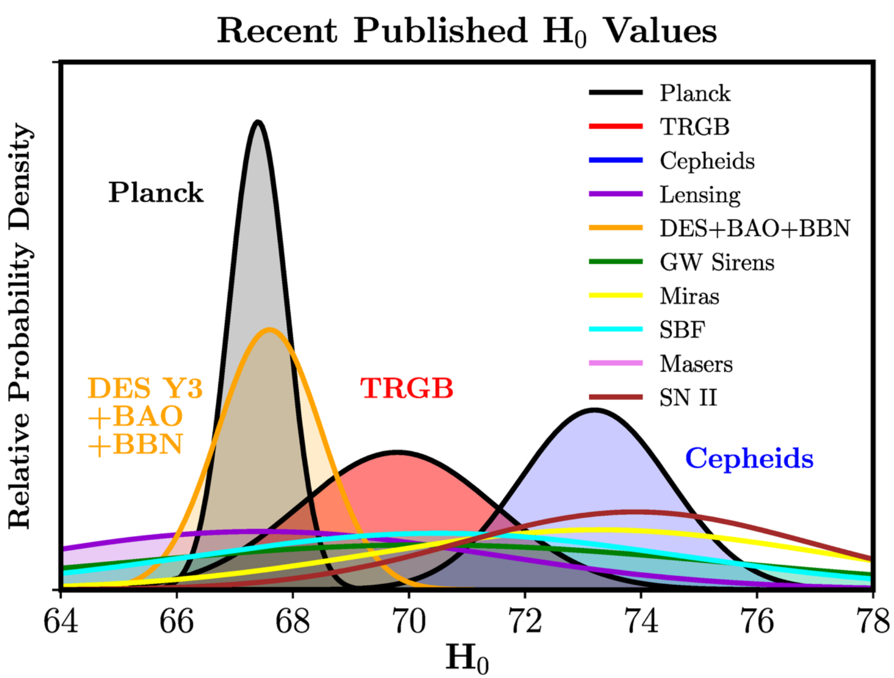

Freedman ApJ 919 (2021) 16 [2106.15656]

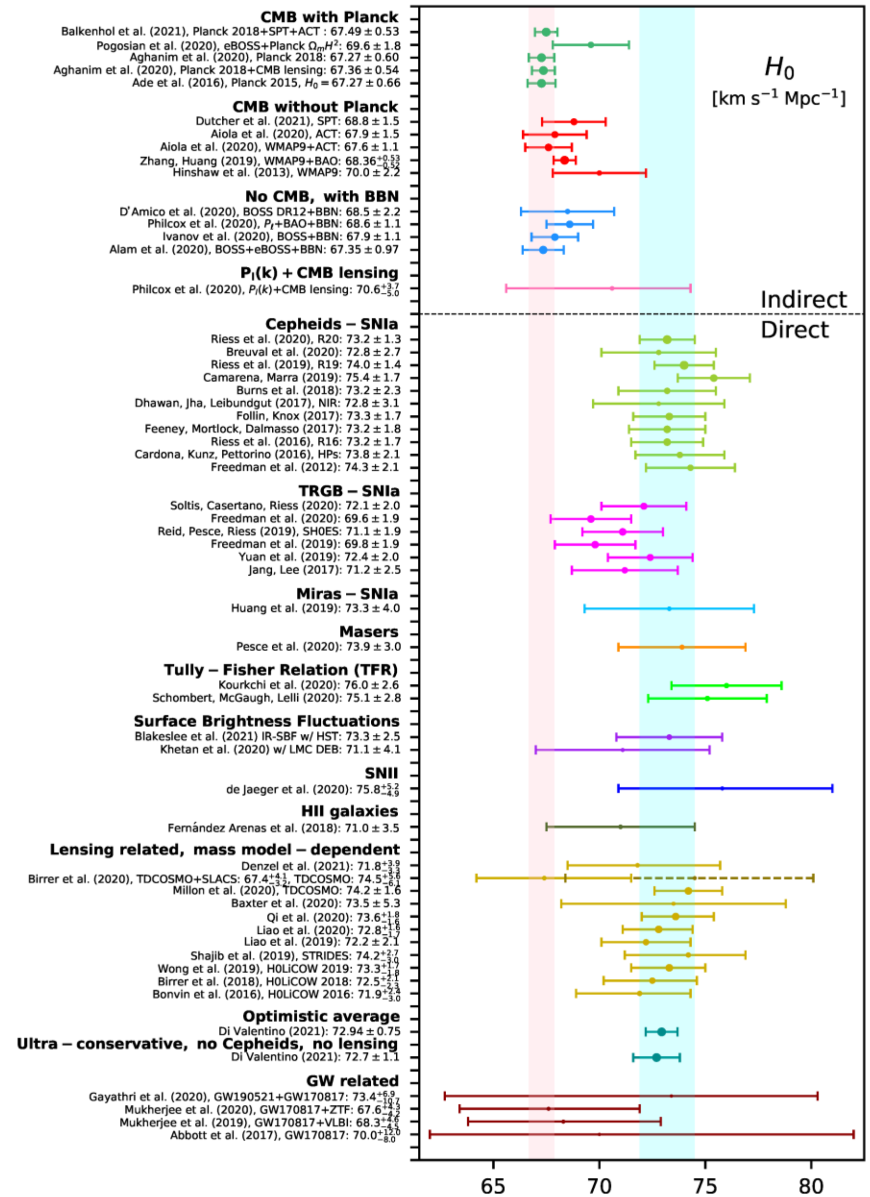

Di Valentino+ arXiv:2103.01183

White Dwarfs

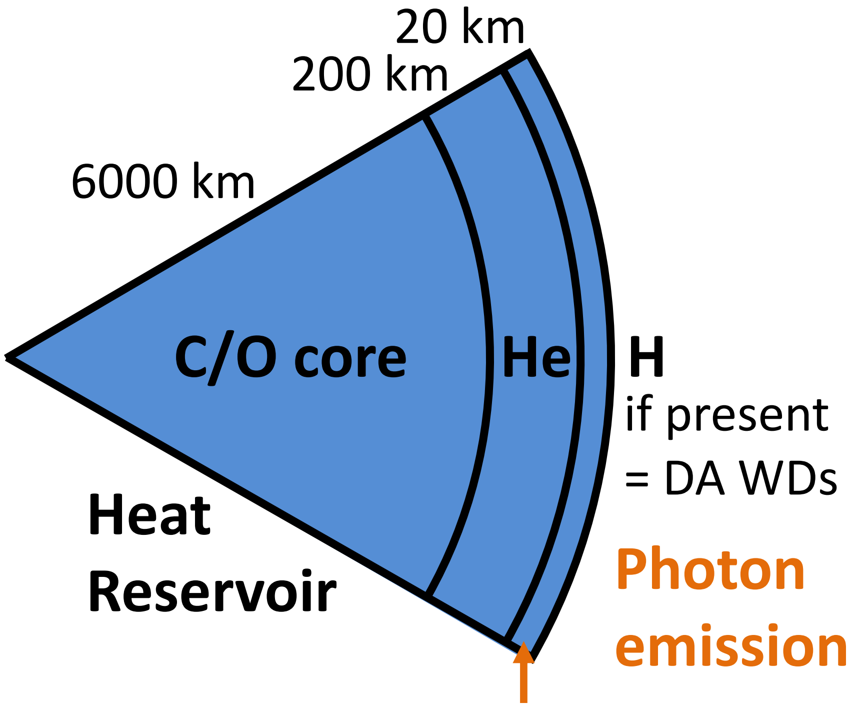

Energy flux control

Cooling much slower for DA type (with H layer)

$R \simeq 6000$ km (Size of the Earth)

$T_{\rm eff} \simeq 10{,}000\text{–}30{,}000\,{\rm K}$ (Sun 6000 K)

$L \simeq 10^{-4}\text{–}10^{-1} L_\odot$

$M \simeq 0.5\text{–}0.8 M_\odot$

$\rho \simeq 10^6 {\rm g/cm^3}$ (very degenerate)

White Dwarf Luminosity Function (WDLF)

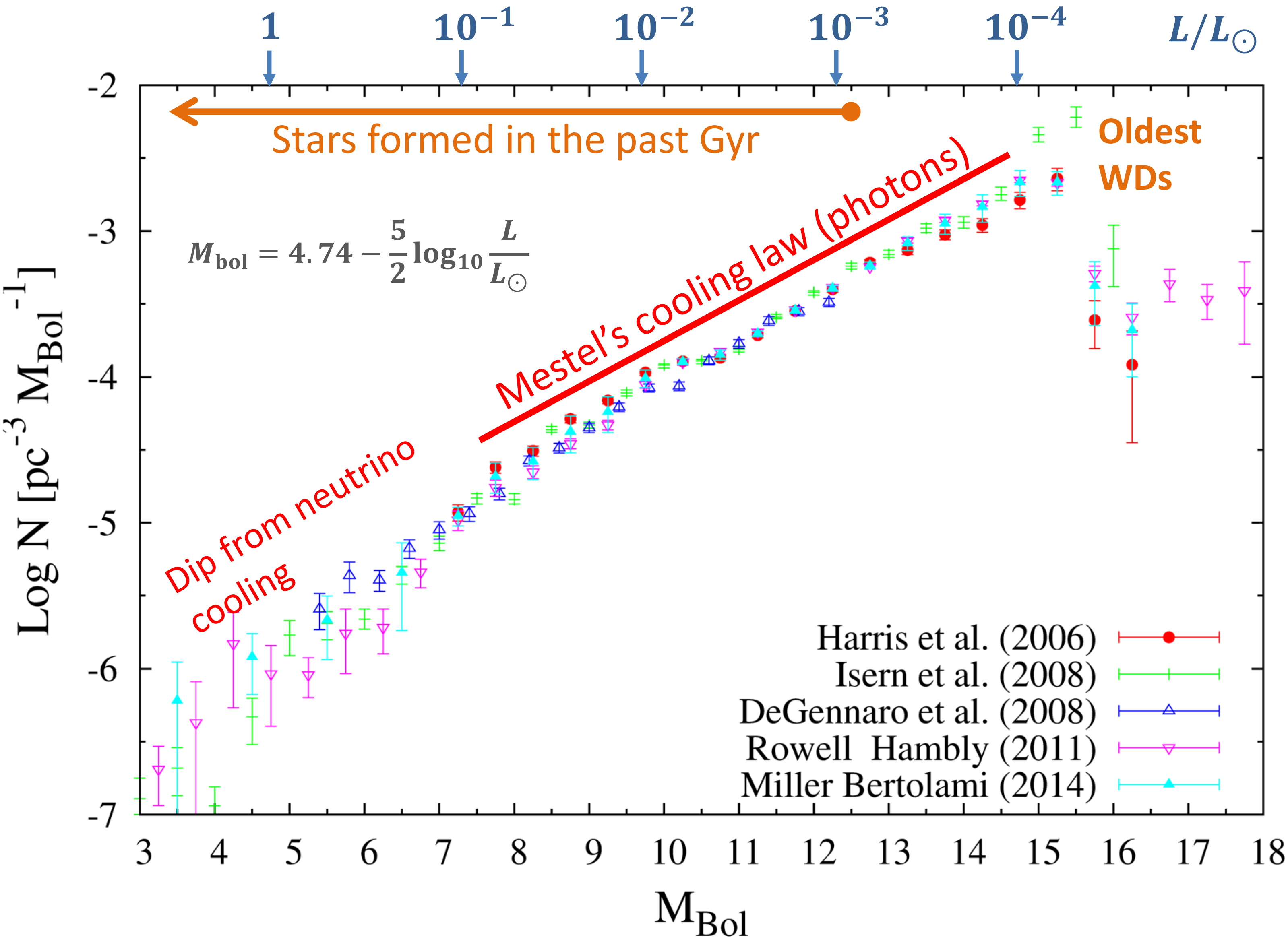

Miller Bertolami, Melendez, Althaus & Isern, arXiv:1406.7712

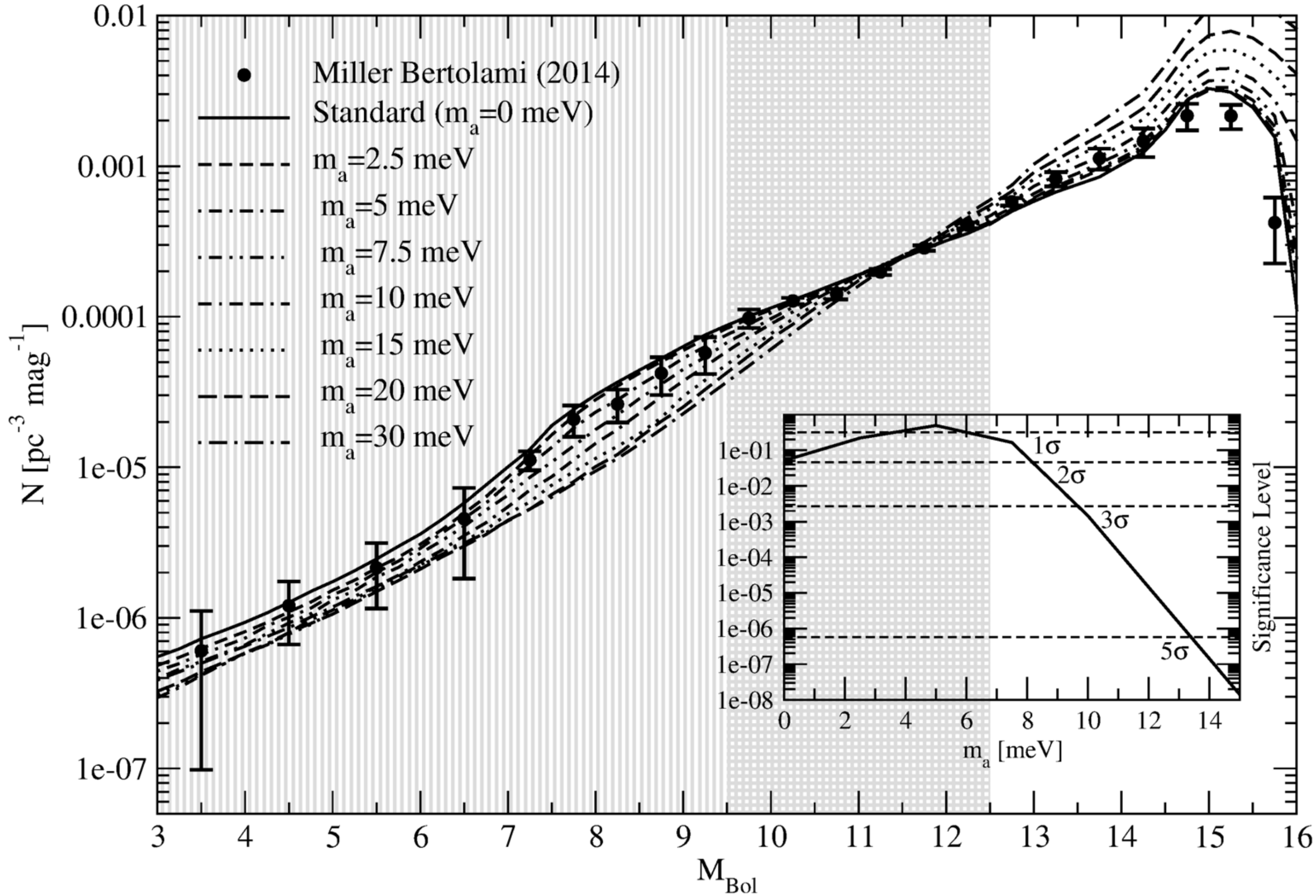

Limits on axion-electron coupling and mass limit in DFSZ model:

$g_{ae} \lesssim 3 \times 10^{-13}$ $m_a \cos^2\beta \lesssim 10\ \mathrm{meV}$

Miller Bertolami, Melendez, Althaus & Isern, arXiv:1406.7712, 1410.1677

For extensions and review see: Isern, arXiv:2002.08069

Pulsating Stars

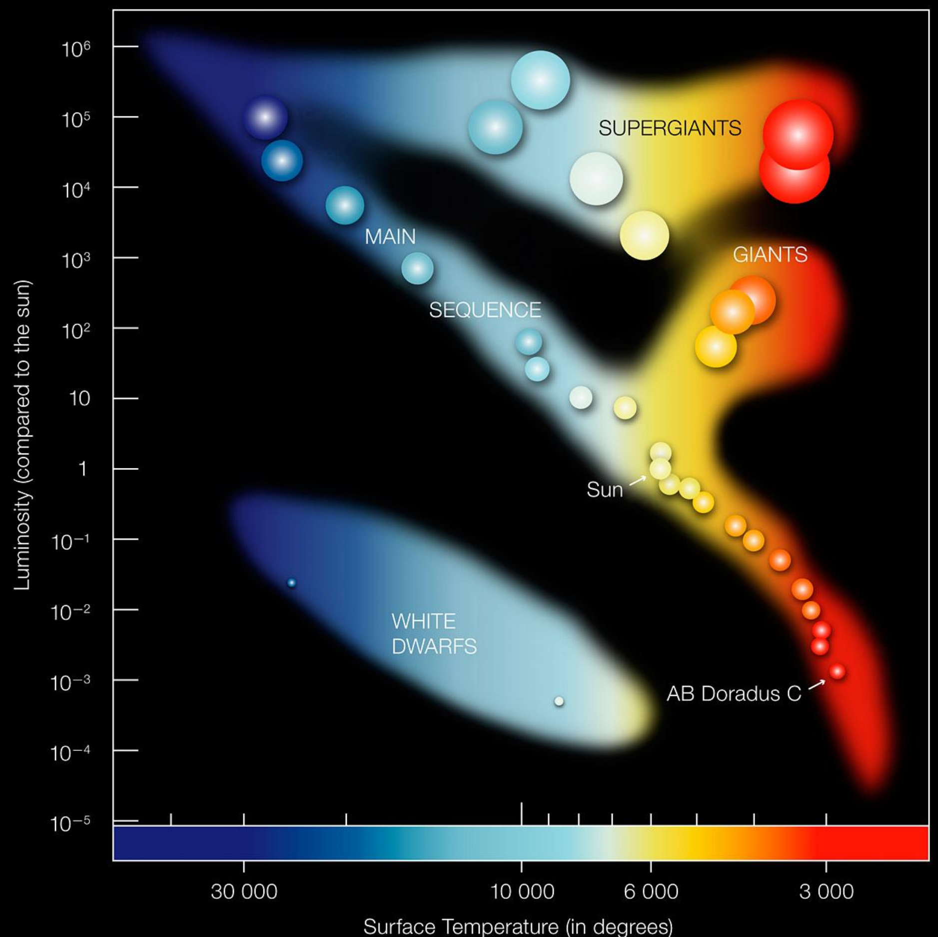

https://www.eso.org/public/images/eso0728c/

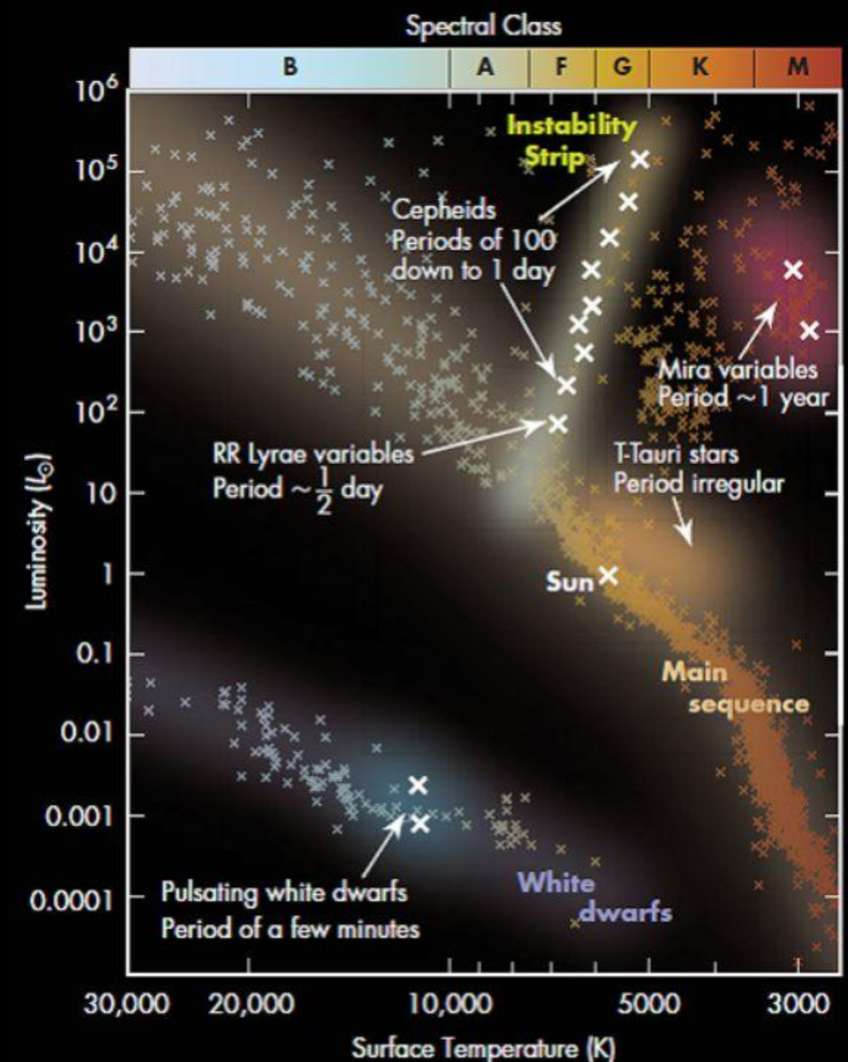

https://scienceatyourdoorstep.com/2021/01/04/what-are-variable-stars/

Non-Radial g-Modes

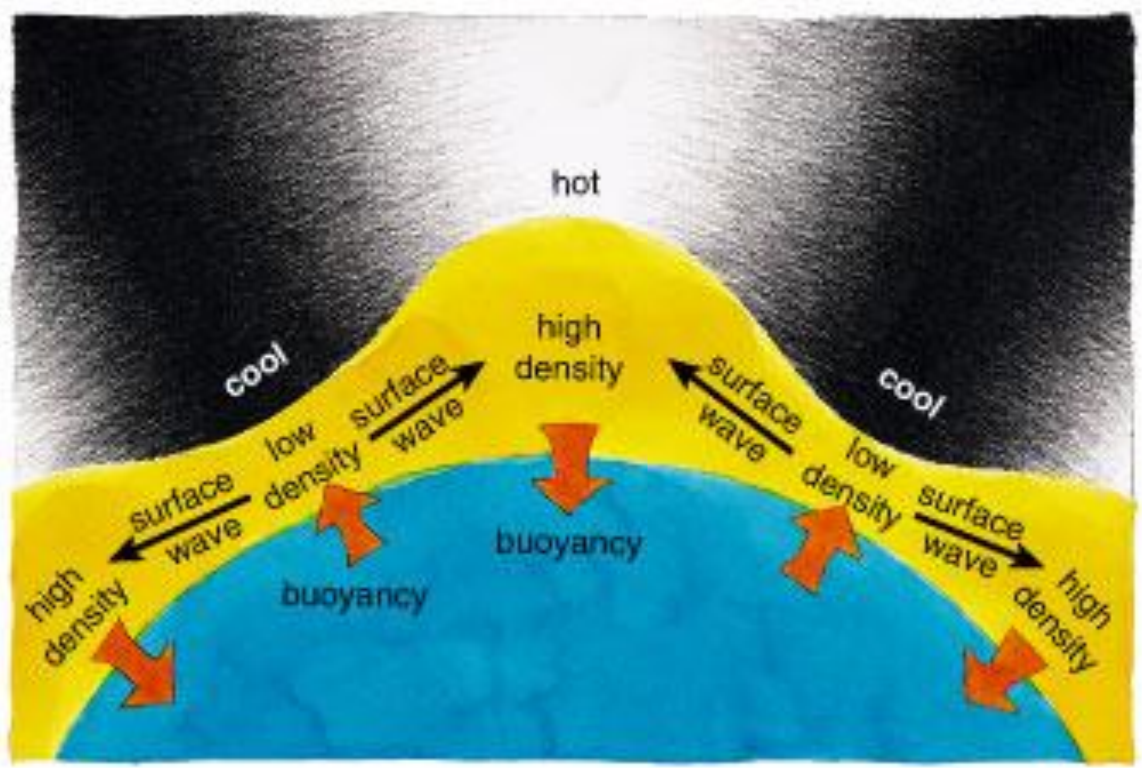

From a talk by J. Isern

$$\frac{d \log \Pi}{dt} \propto -\frac{d \log T}{dt}$$

- Long period waves (100 – 1000 s)
- Gravity is the restoring force

- Period decreases as the star cools
- Characteristic rate 10^{-15} s/s
- Measures cooling speed of a single star

Pulsating White Dwarf G117–B15A

Kepler+ ApJ 254 (1982) 676

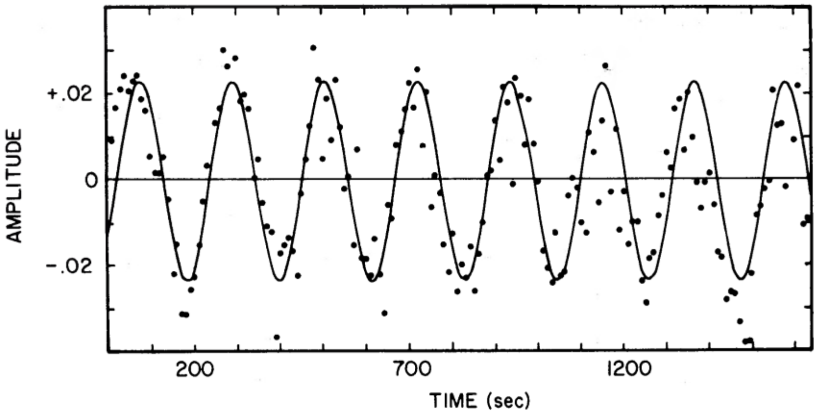

FIG. 1.—A portion of the light curve of G117−B15A in unfiltered light during run 2075. The light curve has been normalized so that the time-averaged brightness of G117−B15A is equal to 1.00, and then 1.00 has been subtracted from the light curve. The solid line is a sine curve with a period of 215.19 s and a semiamplitude of 0.022 mag.

$D = 57.5 \pm 0.1$ pc
$T = 12{,}400$ K
$M = 0.69\, M_\odot$
Period 215.2 s

Kepler+ ApJ 906 (2021) 7

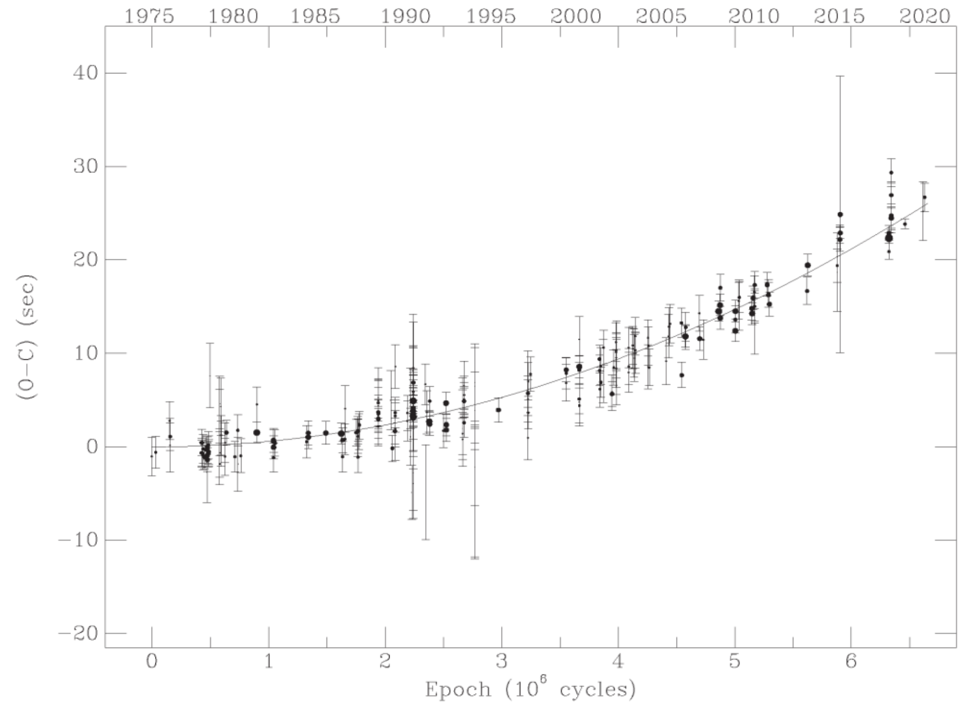

Figure 1. ($O - C$): observed minus calculated times of maxima for the 215 s pulsation of G 117-B15A. The size of each point is proportional to its weight, i.e., inversely proportional to the uncertainty in the time of maxima squared. We show $\pm 1\sigma$ error bars for each point, and the line shows our best-fit parabola to the data. The fact that the line does not overlap these error bars is a demonstration that they are underestimated. Note that as the period of pulsation is 215.1973882 s, the observed total change in phase is only 50 deg.

"Most stable optical clock", slipped by 26 s (of 215.2 s period) in 45 years

$$\dot{P}/P = (5.12 \pm 0.82) \times 10^{-15}\ \text{s/s}$$

G117–B15A Period Decrease: Hint for Axion Cooling?

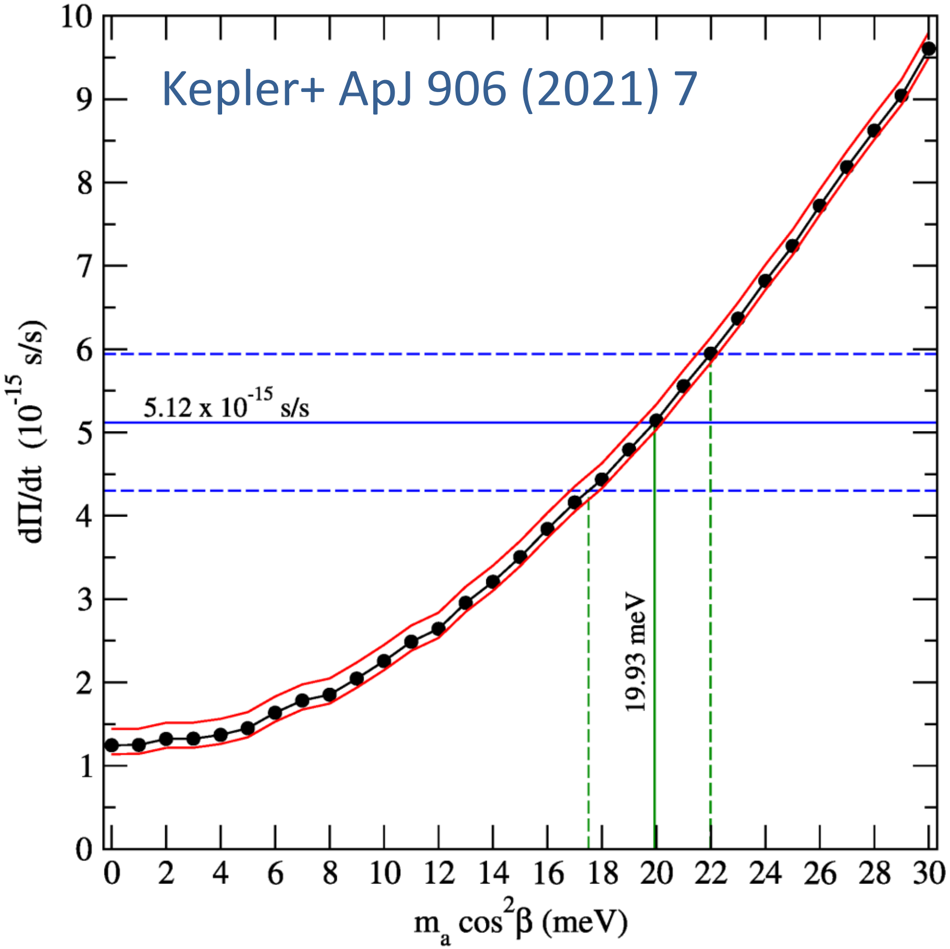

Figure 2. The rate of period change for the mode with $\ell = 1$ and $k = 2$, corresponding to a period of ~215 s in terms of the axion mass (black circles). Dashed lines represent the uncertainties in the value in the observed $\dot{P}$ and the axion mass, while the red curves represent the internal uncertainties in $\dot{P}$ due to modeling.

$$\dot{P}/P = (5.12 \pm 0.82) \times 10^{-15}\ \mathrm{s/s}$$

Emission of axions & friends with direct electron coupling

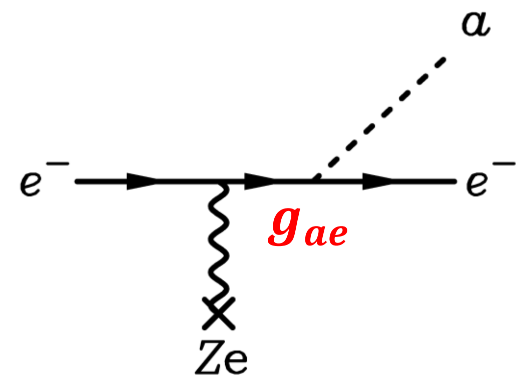

Bremsstrahlung emission by degenerate electrons

Case of DFSZ Axion

$$g_{ae} = 0.28 \times 10^{-13}\ \frac{m_a \cos^2\beta}{\mathrm{meV}}$$

Nominal cooling signal

$$g_{ae} = (5.7 \pm 0.6) \times 10^{-13}$$

Bounds on Axion-Electron Coupling

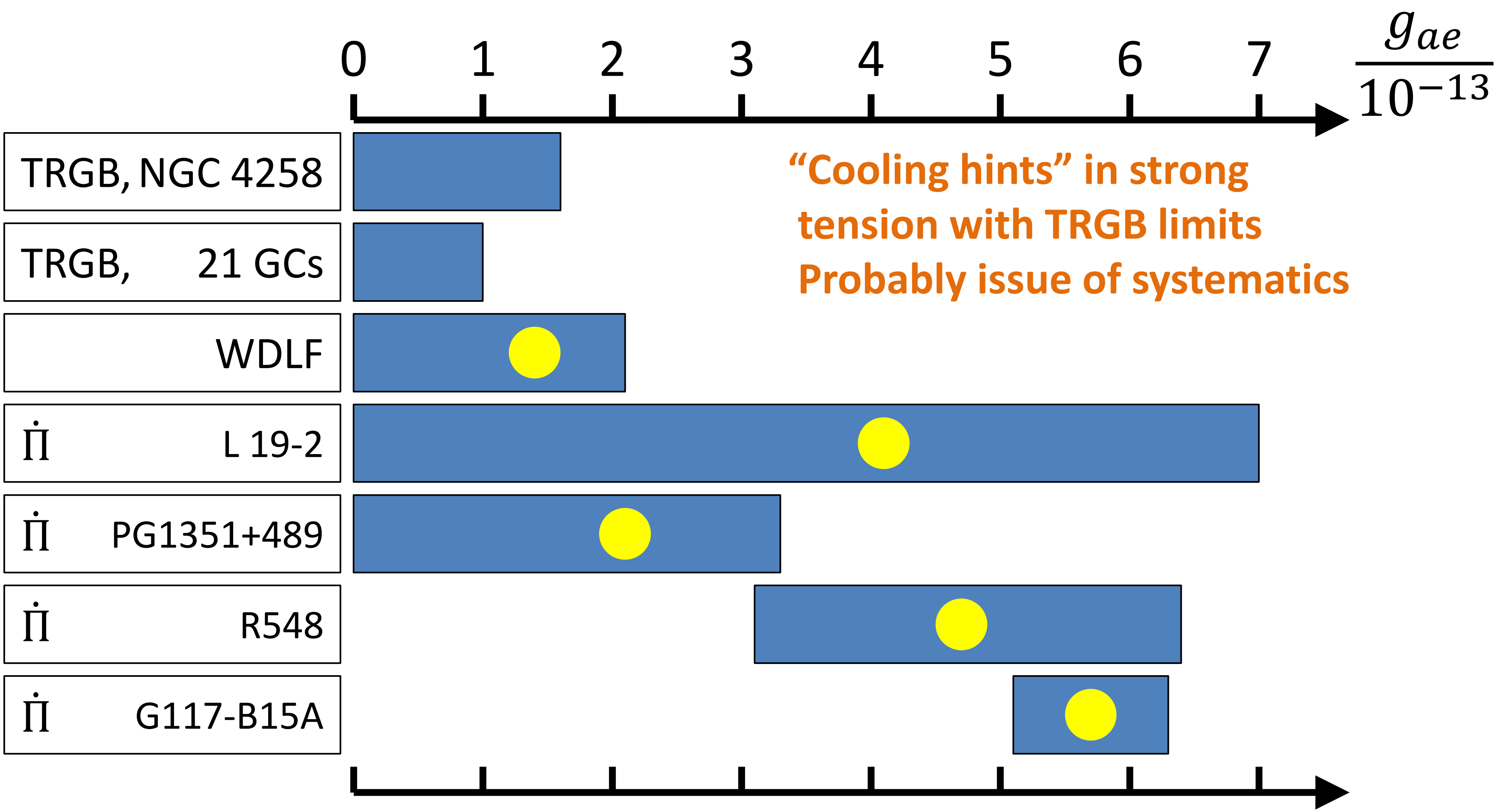

White Dwarfs as Physics Laboratories: Lights and Shadows, arXiv:2202.02052
J. Isern, S. Torres & A. Rebassa-Mansergas
Stellar Evolution Confronts Axion Models, arXiv:2109.10368
L. Di Luzio, M. Fedele, M. Giannotti, F. Mescia & E. Nardi

Astrophysical Axion Bounds

Brand New

The 2024 Edition, Caputo & Raffelt, arXiv:2401.13728, 24 Jan 2024

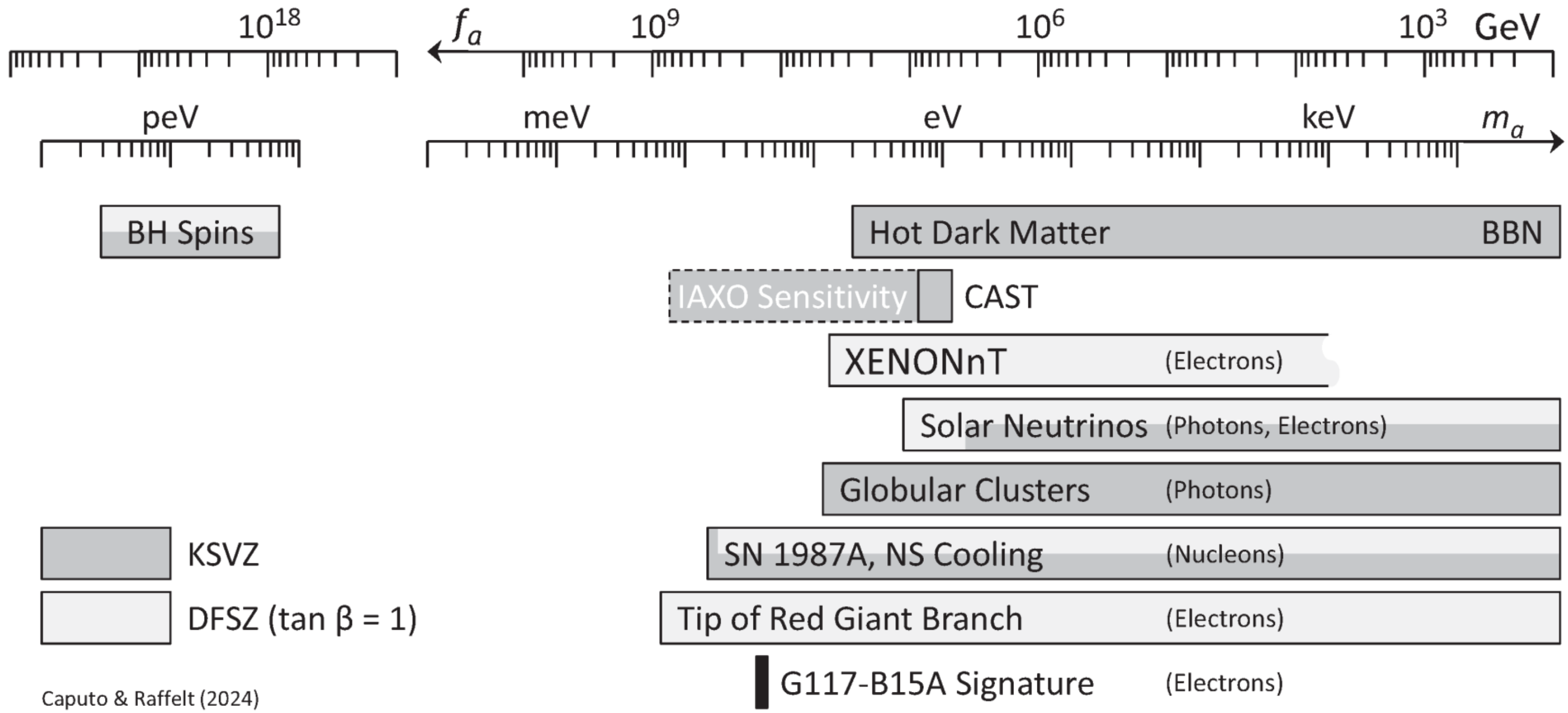

- Many improvements over the years, but overall picture the same
- Specific QCD axion signatures hard to expect from cooling effects
- Best stellar detection opportunity probably (Baby)IAXO


Solar Axions
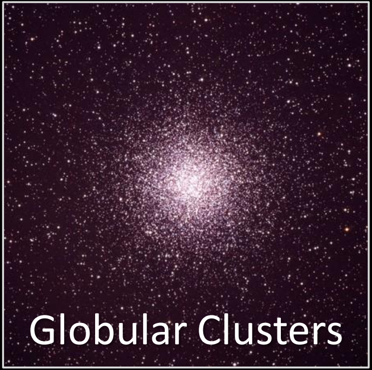
Globular Clusters
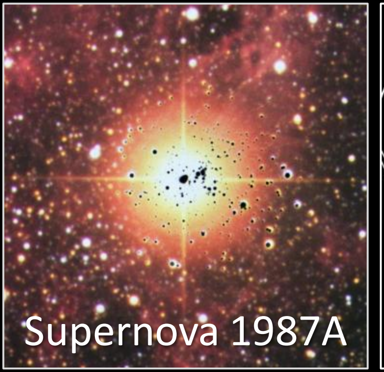
Supernova 1987A
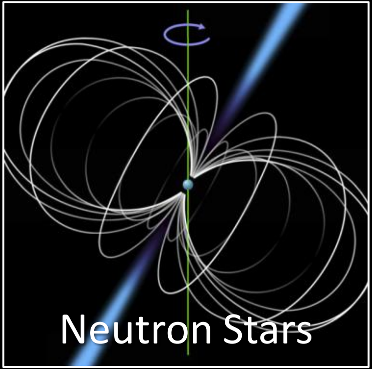
Neutron Stars
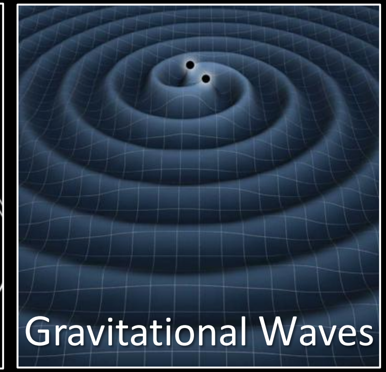
Gravitational Waves

Thanks